A Smooth Permittivity Function for Poisson–Boltzmann Solvation Methods

J. ANDREW GRANT,[1,2] BARRY T. PICKUP,[2] ANTHONY NICHOLLS[3]

[1] *AstraZeneca Pharmaceuticals, Mereside, Macclesfield, Cheshire SK10 4TF, United Kingdom*
[2] *Department of Chemistry, The University of Sheffield, S3 7HF, United Kingdom*
[3] *Openeye Software, Santa Fe, New Mexico*

Received 24 February 2000; accepted 16 November 2000

ABSTRACT: This work introduces a continuous smooth permittivity function into Poisson–Boltzmann techniques for continuum approaches to modeling the solvation of small molecules and proteins. The permittivity function is derived using a Gaussian method to describe volume exclusion. The new method allows a rigorous determination of solvent forces within a grid-based technology. The generality of approach is demonstrated by considering a range of applications for small molecules and macromolecules. We also present a very complete statistical analysis of grid errors, and show that the accuracy of our Gaussian-based method is improved over standard techniques. The method has been implemented in a new code called ZAP, which is freely available to academic institutions.[1]
 J Comput Chem 22: 608–640, 2001

Keywords: solvation; Poisson–Boltzmann; solvent-forces; binding; energies

Introduction

Water plays a dominant role in biology. It affects binding, ionization states, redox potentials, diffusion, catalysis, and conformations of molecules. Any theoretical understanding of life at the molecular level requires an understanding of water. Water's simple molecular structure does not lead to simple molecular mechanics with problems in long-range electrostatics, boundary effects, polarization, and ion correlation. Simulations with water take a long time, and are seldom superior to simpler models.

Approximate models capture average, or "continuum," behavior of water. These theories favor information on water's effect on a solute over information about water itself. The use of solute surface area as a quantitative measure of solubility is a continuum method, as is the Poisson–Boltzmann equation (PBe). A simple heuristic is that surface area accounts for the hydrophobic effect while the PBe estimates hydrophilic energies. Considerable effort is poured into the methodology and application of both approaches because they have proved useful and are much faster than all-atom simulations. This article concerns the PBe and how its efficiency and accuracy can be much improved by

Correspondence to: J. A. Grant; e-mail: andrew.grant@astrazeneca.com

using a smoothly varying dielectric function. Although there are several methods available for solving the PBe, only grid-based methods are capable of handling macromolecules like proteins and DNA. DelPhi,[2, 3] from Barry Honig, is one of the most important examples of a grid-based PBe solver.

The results in this article come from our new multilevel, multigrid solver, ZAP. We wanted ZAP to be a PBe solver that did not suffer from the difficulties associated with grid-based methods. The mapping of molecular volume and charge onto a cubic lattice is an inaccurate representation and leads to an orientational and positional dependence of calculated energies. As lattice spacing grows smaller, this variation decreases, but at the cost of computer memory and time. A common solution is to calculate at coarse grid scales for several orientations. Careful analysis shows that rotationally and translationally averaged values also depend on grid scale. Introducing a dielectric function based on atom-centered Gaussians attacks the root of such problems: the discontinuity of the dielectric at the boundary between solvent and solute. It also provides a physically appealing description of the solute-solvent transition and a simple way to calculate solvent forces. We also wanted to retain the best predictive power of older methods. Therefore, our dielectric model is parameterized to DelPhi small molecule solvation energies. The inclusion of solvent energies and forces in the conformational analysis of drug-sized molecules is important, but the model also works for proteins. Comparisons are made for protein residue desolvation energies, binding of small ligands and the pKa of ionizable residues. Calculating solvation contributions to protein–ligand binding is a challenge of the PBe approach. The discrete dielectric model has tight-binding polar molecules trading aqueous solvation for protein solvation so that the net contribution is close to zero. Precision is vital because the net energy is the difference of large numbers. Precision and large molecules mean calculations that run from minutes to hours. The Gaussian based dielectric model predicts the same effect in a few seconds.

Methods

THE POISSON–BOLTZMANN EQUATION

Continuum models of the electrostatic effects of solvent and electrolytes make use of a combination of classical electrostatics and Debye–Hückel theory. The earliest treatment of such models[4–6] considerably predates conventional molecular mechanics techniques. Current approaches based on numerical solutions to a discretized PBe are widely used. The PBe models solute as a region of low permittivity [$\epsilon(\mathbf{r})$] containing a set of distributed point charges. Aqueous solvent becomes a region of high permittivity that may contain dissolved electrolyte. Appendix A reviews aspects of the PBe and the discretization process that are relevant to our proposed modifications.

Describing the boundary between high and low dielectric is critical. An example is the Van der Waals surface (VDWS), which is the surface of the molecule where each atom is represented by a sphere of appropriate radius. More commonly used is the molecular surface (MS),[7] defined to be the inner surface smoothly traced by a probe sphere as it rolls these atomic spheres. The probe radius is typically set to 1.4 Å, half water's mean oxygen–oxygen distance. Although more complex, the molecular surface has several advantages over the VDWS. It is smoother, avoiding the cusps that form at the intersections of atomic spheres. It excludes high permittivity from regions a water molecule could not penetrate, which makes little difference for small molecules, but becomes important for proteins. An alternative to the MS for proteins is the accessible surface (AS),[8] which is equivalent to the VDWS, where each atom has its radius increased by 1.4 Å. The AS is easier to calculate, simplifies solvent force evaluations, excludes water from protein interiors, and meets a perceived need in reducing the desolvation penalty calculated for molecular association. However, it does not correctly predict the solvation energies of small molecules. Because such predictions are the strongest validation of PB theory the molecular surface remains the more widely used. A recently proposed alternative surface is the isovalue contour (IVC) of a Gaussian-based volume function.[9]

The problems associated with surface-derived permittivity functions are both physical and algorithmic. The fundamental physical issue is that macroscopic properties must vary continuously. Any description of the permittivity changing instantaneously from one point to another is incorrect, though possibly still useful. The widely used molecular surface has an additional unpleasant characteristic: the infinitesimal movement of a single atom can produce large surface changes. A practical example is the small shift of a bound ligand suddenly excluding a water molecule, dramatically changing the predicted binding energy (see Fig. 1).

Algorithmic issues are fourfold: implementation, convergence, discretization, and gradients. Imple-

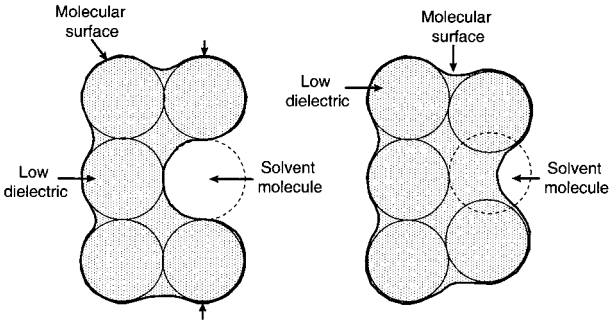

FIGURE 1. Schematic illustration of instabilities in the molecular surface method for defining dielectric boundaries. The solvent pocket in the left diagram collapses due to small atomic displacements (see vertical arrows).

mentation issues are most severe for the molecular surface, which is difficult to construct rapidly. Finite-element[10, 11] or boundary-element[12–14] methods both suffer time penalties to tesselate either molecular or iso-value surfaces.

Convergence issues are often overlooked but can be serious. The normally robust method of successive overrelaxation[15] employed in DelPhi can be broken by setting the external permittivity too large. Multigrid methods, while efficient, are sensitive to discrete boundaries, usually requiring harmonic averaging of permittivity values to ensure convergence.[16, 17] It is a characteristic of iterative numerical methods that they converge slower the more discrete the boundary.

In grid-based solutions to the PBe it is necessary to discretize physical values onto a grid (see Appendix A). A value at a grid point is supposed to represent physical properties in that region. The coarser the grid, the more poorly a single point can model the local volume and the more inaccurate the energies predicted. Because the mapping depends on the orientation and position of the molecule relative to the grid, both affect the grid description and both cause variation in calculated energies. The more rapidly the physical quantites vary, the greater the difficulties of any grid-based approach. Surface derived permittivity functions are therefore particularly badly behaved.

The calculation of derivatives of grid-based physical quantities is essential for robust and rapid calculation of solvent forces. The dielectric discontinuity introduced by surface models makes such an evaluation difficult, and has hampered the inclusion of solvent effects from the PBe into modelling packages.

Discretization problems associated with surface derived permittivity functions have been known for some time. Davis et al.[18] took an innovative approach that harmonically averaged the permittivity function over a single grid spacing. They observed better stability of calculated energies with respect to grid scale and spacing. However, the model still attempts to calculate the energies of the discrete boundary model. *Ad hoc* smoothing procedures as shown by Sharp et al.[19] can be used near the boundary. They work reasonably well, but are complicated and inefficient, and do not admit efficient computation of solvent forces.

SMOOTH DIELECTRIC AND IONIC MAPS

This section introduces our new method of describing the variation of the permittivity for a solute in a continuum solvent. The aim is to replace the discontinuous dielectric boundary arising from a hard sphere description of atoms. The central idea uses a function that smoothly maps out the excluded volume of a molecule. Each atom is described by a Gaussian, and these are combined using a composite molecular function that can be used to calculate volumes, and their respective nuclear coordinate derivatives.[20, 21] The dielectric map function that we are seeking describes a smooth variation of dielectric from low values inside the solute to high values in bulk solvent. We require a way in which we can connect a conventional hard sphere of radius σ_A with our Gaussian representation. This is achieved by insisting that the Gaussian has the same volume as the hard sphere in question. A Gaussian of nominal radius σ_A is given by

$$\rho_A^g(\mathbf{r}) = p_A \exp\left(-\kappa r_A^2/\sigma_A^2\right) \tag{1}$$

where p_A is a height factor, r_A is the radial distance from atom A, and κ is a dimensionless exponent. The volume integral is

$$V_A = \int d\mathbf{r}\, \rho_A^g = p_A \left(\frac{\pi}{\kappa}\right)^{3/2} \sigma_A^3 \tag{2}$$

where $d\mathbf{r}$ is a volume element, and the integral is taken over all space. The integration in (2) is carried out using the standard formula for a Gaussian. It follows from (2) that the constraint

$$p_A \left(\frac{\pi}{\kappa}\right)^{3/2} = \frac{4}{3}\pi \tag{3}$$

is required to obtain the equivalent hard sphere volume. Borrowing from the analogous hard sphere[22]

case, we can now write a molecular function

$$\rho_{mol}(\mathbf{r}) = 1 - \prod_A (1 - \rho_A^g) \tag{4}$$

in terms of a repeated product over atomic terms. Expanding this expression we obtain

$$\begin{aligned}\rho_{mol}(\mathbf{r}) &= \sum_A \rho_A^g - \sum_{A>B} \rho_A^g \rho_B^g + \sum_{A>B>C} \rho_A^g \rho_B^g \rho_C^g + \cdots \\ &= \rho_{sum}(\mathbf{r}) + \text{“intersection terms”}\end{aligned} \tag{5}$$

where $\rho_{sum}(\mathbf{r})$ is the linear summation of all atomic terms, and the higher products represent corrections for over or undercounting of atomic intersections. In previous work[20, 21] this formulation (5) was used together with a parameterised value of p_A (and hence κ), using (3) to give highly accurate values of molecular volumes and areas. During the course of this and related work,[23] experimentation with a number of dielectric mapping functions using (5) to describe the solute molecule, demonstrated that linear switching related to $\rho_{mol}(\mathbf{r})$ produced dielectric functions that increase towards solvent values far too rapidly with distance from atomic centers. These trial dielectric functions were tested using the algebraic MultiGrid code, pmg, developed by Michael Holst at Caltech. These functions also produced undesired patches of high dielectric inside proteins, in regions that are sterically inaccessible to water (akin to using the van der Waals surface to describe dielectric boundaries). A simple function describing the spatial variation in the permittivity having the correct properties is of the form

$$\begin{aligned}\epsilon(\mathbf{r}) &= \epsilon_{solute} + (\epsilon_{solvent} - \epsilon_{solute}) \exp\bigl(-A\rho_{sum}(\mathbf{r})\bigr) \\ &= \epsilon_0\bigl[\epsilon^r_{solute} + \bigl(\epsilon^r_{solvent} - \epsilon^r_{solute}\bigr) \exp\bigl(-A\rho_{sum}(\mathbf{r})\bigr)\bigr]\end{aligned} \tag{6}$$

where A is a suitable constant. The quantity ϵ_0 is the permittivity of the vacuum, and ϵ^r_{solute}, $\epsilon^r_{solvent}$, are the dimensionless relative permittivities of the solute and solvent, which are referred to henceforth as “dielectric constants.” Calculated values of $\epsilon(\mathbf{r})$ on a grid are subsequently referred to as a dielectric map. The purpose of the extra exponentiation is to (a) smooth out variations of ϵ inside large molecules; and (b) produce a smooth transition from solute to solvent at the molecular boundary.

The essential feature of (6) is that the Gaussian representation is used as the method for smoothly delineating the excluded volume of the molecule. ρ_{sum} can be used rather than the full expression (5), because the additional exponentiation in (6) smooths out the extra shape detail provided by the intersection terms. The variation of (6) compared to the variation of a single Gaussian is shown in Figure 2. Gaussian volume exclusion has also been used by Schaefer and Karplus[24] in the context of a Generalized Born[25] method. A volume exclusion function with atomic piecewise polynomials has also been used by Im et al.[26] for the PBe.

The evaluation of the salt term and its derivatives requires an explicit function $\lambda(\mathbf{r})$, which can be mapped onto grid points as required by (56) of Appendix A. We use the expression

$$\lambda(\mathbf{r}) = \exp\bigl(-A\rho^{stern}_{sum}\bigr) \tag{7}$$

where the constant A is identical to that used for dielectric switching, but

$$\rho^{stern}_{sum} = \sum_A \rho_A^{g,stern} \tag{8}$$

where the individual Gaussians of the summation have radii given by

$$\sigma_{A,stern} = \sigma_A + \sigma_{stern} \tag{9}$$

where σ_{stern} is the depth of the Stern layer. This has the advantage that is produces a switching function which maps directly into the dielectric analogue as $\sigma_{stern} = 0$. Although the outline of a formalism treating ionic terms has been presented, in the present work we do not implement it in terms of practical computation. The expressions are shown to emphasise the generality of our approach to the introduction of continuous functions into Poisson–Boltzmann grid-based technology. We intend to implement the ionic terms in future work, although it has been noted by Gilson[27] that force terms arising from the ionic boundary are small at physiological pH, when computed using linear versions of the PBe.

The functions that we have defined for dielectric and ionic maps need to be evaluated on the rectangular grid used in the PB calculations. The mathematical properties of Gaussians are such that this process is computationally very efficient.

SMOOTH CHARGE DISTRIBUTIONS

The discretized PBe described in Appendix A contains the following grid cell integral

$$q_{ijk} = \int_{V_{ijk}} d\mathbf{r}\, \rho_{mol}(\mathbf{r}) \tag{10}$$

which is simply the total charge contained within the grid cell *ijk*. In principle a continuous density $\rho_{mol}(\mathbf{r})$ can be obtained from a quantum-mechanical method. In such cases the cell integral (10) is a smooth function relative to the grid, and differentiability with respect to atomic coordinates is not a

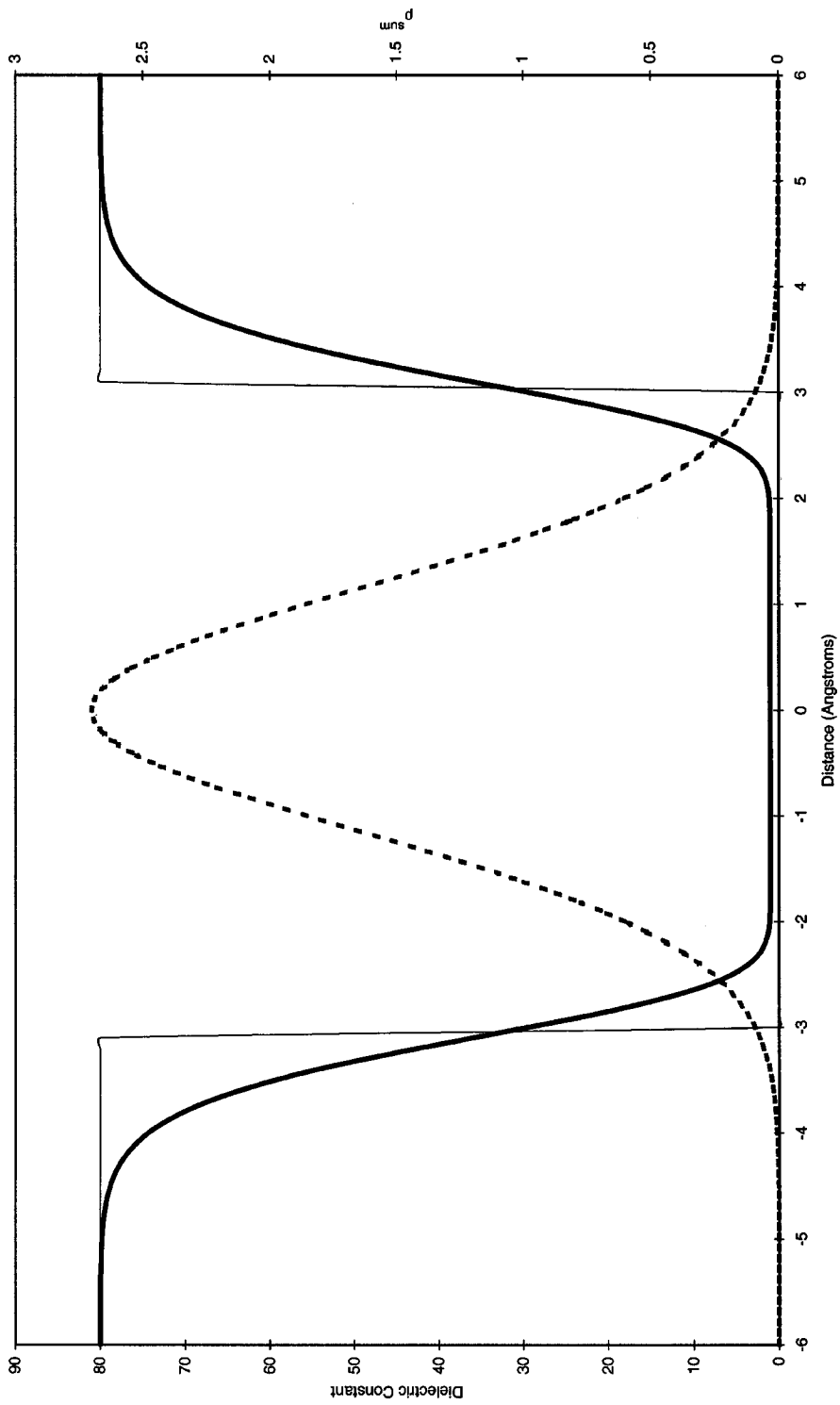

FIGURE 2. A cross-section of the relative permitivitty of an atom of radius $\sigma = 2.5$ Å using $A = 11.8$ (thick line). The underlying atomic Gaussian density function (broken line) and discrete dielectric boundary are also shown.

problem, even if the integration is not completely straightforward. However, in most applications, the charge distribution $\rho_{mol}(\mathbf{r})$ is described in terms of a set of N atom centred "point" charges, thus:

$$\rho_{mol}(\mathbf{r}) = \sum_{i=1}^{N} q_i \delta(\mathbf{r} - \mathbf{r}_i) \tag{11}$$

It is necessary, therefore, to obtain a simple and consistent scheme for distributing atomic charges onto the grid, which ideally has the following properties: (a) computational efficiency; (b) the computed grid charges q_{ijk} must be represented by formulae, which can be analytically differentiated with respect to atomic coordinates, to compute solvent forces; (c) a hierarchy of approximations with a consistent mathematical formalism leading to increased accuracy with respect to errors arising from orientational and positional dependence of the molecule to the grid; and (d) provide a good representation of the underlying charge distribution, in particular conservation of charge and dipole moment.

Conventional schemes for distributing atomic charge distributions onto grids rely on some form of linear inverse interpolation.[15, 26, 28] Although efficient, we found such schemes when combined with the smooth dielectric maps described previously, gave rise to unacceptably large orientational errors in computed small molecule solvation energies. In addition, linear inverse-interpolation schemes possess discontinuities in first-order positional gradients, and because of this are problematic when used to compute analytic PB solvent forces. An alternative approach for obtaining grid-based charge distributions, is to combine a uniform charging method,[29] with an antialiasing algorithm.[19] However although conceptually straightforward and very accurate in reducing grid errors, this scheme is computationally expensive, and not particular suitable for obtaining analytical derivatives. In this work we make use of a simple quadratic inverse-interpolation scheme to distribute charges onto the grid, which is continuous up to first derivatives.

The details of this scheme are given in Appendix B.

SOLVENT FORCES

The introduction of smooth dielectric and charge mapping functions that are differentiable gives rise to the possibility of using an analytic approach to calculate solvent forces, i.e., the force on a nucleus due to solvent electrostatic polarization. The following methodology is based upon techniques widely used in quantum chemistry for the calculation of analytic derivatives.[30] The derivation begins from the matrix notation for the discrete PBe described in Appendix A.

$$\mathbf{A}\boldsymbol{\Phi} = \mathbf{q} \tag{12}$$

where $\mathbf{A}$ is a $N \times N$ matrix, and $\boldsymbol{\Phi}$ and $\mathbf{q}$ are $N \times 1$ vectors, $N = n_1 n_2 n_3$, is the total number of grid points, n_1, n_2, and n_3 are the $x-, y-, z-$ direction grid dimensions.

The elements of the matrix $\mathbf{A}$ are described in Appendix A. The electrostatic energy of the system can be written as written as

$$E = \tfrac{1}{2}\mathbf{q}^{\dagger}\boldsymbol{\Phi} \tag{13}$$

There are two straightforward techniques for the extraction of solvation energies from (13). One is a method involving an additional calculation with a uniform solute dielectric, and the other is based upon an interpolation and table lookup of the integrated Green's function for the electrostatic potential in a uniform dielectric.[31] Both of these procedures eliminate the self-energy and finite-difference approximation to Coulombic interaction energy, leaving only the solvation energy. We will analyze the electrostatic forces using the total energy that appears in (13), but observe that it is straightforward to apply one of the two previously described techniques to obtain the actual solvation force.

It is important to observe that the quantities $\mathbf{A}$ and $\mathbf{q}$ depend on the atomic coordinates. We denote this by writing $\mathbf{q}(R)$, $\mathbf{A}(R)$, where R is a single structural parameter with respect to which we wish to obtain a derivative. For example, R could represent an atomic radius, or a coordinate of an atom. It follows that the solution $\boldsymbol{\Phi} = \boldsymbol{\Phi}(R)$, and the energy $E = E(R)$. Expanding the relevant quantities in terms of a Taylor series, for example for A as follows:

$$\mathbf{A}(R + \delta R) \approx \mathbf{A}(R) + \frac{d\mathbf{A}(R)}{dR}\delta R + \cdots \tag{14}$$

For conciseness we now adopt a perturbation theory notation:

$$\mathbf{X} = \mathbf{X}^{(0)} + \mathbf{X}^{(1)} + \cdots \tag{15}$$

where the quantity $\mathbf{X}$ can be equal to $\mathbf{A}$, q, $\boldsymbol{\Phi}$, or E. The zeroth-order quantities are all evaluated at the original geometry, and the first-order quantities represent the 1st derivatives. The theory is correct for *any* parameter for which $\mathbf{A}$, $\mathbf{q}$ are analytically differentiable. The zeroth-order equation

$$\mathbf{A}^{(0)}\boldsymbol{\Phi}^{(0)} = q^{(0)} \tag{16}$$

is the standard PBe (at R) which we assume has already been solved. Substitution of (15) into (12) and

collecting terms gives the first-order equation

$$\mathbf{A}^{(0)}\boldsymbol{\Phi}^{(1)} + \mathbf{A}^{(1)}\boldsymbol{\Phi}^{(0)} = q^{(1)} \tag{17}$$

which has the formal solution

$$\boldsymbol{\Phi}^{(1)} = \left(\mathbf{A}^{(0)}\right)^{-1}\left[q^{(1)} - \mathbf{A}^{(1)}\boldsymbol{\Phi}^{(0)}\right] \tag{18}$$

However, we do not require to solve this equation if we only require the first-order electrostatic energy

$$E^{(1)} = \tfrac{1}{2}\left[q^{(0)\dagger}\boldsymbol{\Phi}^{(1)} + q^{(1)\dagger}\boldsymbol{\Phi}^{(0)}\right] \tag{19}$$

This is clear by substituting (18) into (19) to get

$$E^{(1)} = \tfrac{1}{2}\left[q^{(0)\dagger}\left(\mathbf{A}^{(0)}\right)^{-1}\left(q^{(1)} - \mathbf{A}^{(1)}\boldsymbol{\Phi}^{(0)}\right) + q^{(1)\dagger}\boldsymbol{\Phi}^{(0)}\right] \tag{20}$$

We note that (16) has the formal solution

$$\boldsymbol{\Phi}^{(0)} = \left(\mathbf{A}^{(0)}\right)^{-1}\mathbf{q}^{(0)} \Leftrightarrow \boldsymbol{\Phi}^{(0)\dagger} = \mathbf{q}^{(0)\dagger}\left(\mathbf{A}^{(0)}\right)^{-1} \tag{21}$$

and because $\mathbf{A}^{(0)}$ is hermitian [see Appendix A, eq. (59)] it follows that

$$E^{(1)} = \left[\boldsymbol{\Phi}^{(0)}q^{(1)} - \tfrac{1}{2}\boldsymbol{\Phi}^{(0)\dagger}\mathbf{A}^{(1)}\boldsymbol{\Phi}^{(0)}\right] \tag{22}$$

Equation (22) contains the three terms previously described by Gilson et al.[27] The $\boldsymbol{\Phi}^{(0)}q^{(1)}$ term in (22) represents the interaction of perturbed charges with the unperturbed Poisson–Boltzmann potential. It can be shown that this is equivalent to the interaction of the unperturbed charges with the electric field at each charge, referred to by Gilson et al.[27] as "$q\mathbf{E}$ forces." The second term in (22) can be understood by examining the $\mathbf{A}$ matrix elements in eq. (58), of Appendix A. $\mathbf{A}$ is linear in both the dielectric $\epsilon(\mathbf{r})$ and the ionic screening factor $\lambda(\mathbf{r})$. It follows that the gradient term $\mathbf{A}^{(1)}$ is linear in the gradients of $\epsilon(\mathbf{r})$ and $\lambda(\mathbf{r})$ and, hence, we can interpret this term as Gilson's dielectric and ionic boundary "pressure" terms. In our case, there is no boundary, but instead, we have regions equivalent to dielectric and ionic boundaries where the gradients $\nabla\epsilon(\mathbf{r})$ and $\nabla\lambda(\mathbf{r})$ are large. It should be emphasized that solvation force calculations using (22) can be carried out without any additional iterative solutions of the PBe. The quantities in (22) are constructed by explicit differentiation at grid points of the ϵ and λ maps given in eqs. (6) and (7). These derivatives are trivial to obtain given Gaussian representations of the solute–solvent dielectric and ionic transition regions. In counterdistinction, methods using hard-sphere dielectric and ionic maps give rise to severe difficulties because of the inability to find simple formulations of the gradients of these maps. This expression only involves the solution of the electrostatic potential ($\boldsymbol{\Phi}^{(0)}$) to zeroth-order. The other quantities $\mathbf{q}^1$ and $\mathbf{A}^1$ are derivatives of the previously defined matrix elements. This is just a version of the "$2n + 1$" order rule in quantum chemistry perturbation theories,[30] where the manipulation involving (21) is known as the turnover rule.[30]

Results

We present a range of applications of the Gaussian PB model and consider the results with respect to data obtained using the conventional molecular surface description of the dielectric boundary. In the following sections the abbreviations G and MS denote the Gaussian and Molecular Surface dielectric models, respectively. Where relevant specific values of ϵ^r_{solute} and $\epsilon^r_{solvent}$ are given in accompanying parenthesis. The code used to explore the Gaussian and other dielectric models described in this article is part of the ZAP object library that is freely available to academic institutions. Written in C, ZAP follows a toolkit paradigm popularized by Daylight Chemical Information Systems, that uses opaque pointers, also called "handles," to represent procedures, and data structures such as molecules. Functionality is provided by a set of function calls, or "interfaces," which my be easily linked into the user's own code.[1]

MOLECULAR SOLVATION ENERGIES

This section presents results for the computation of molecular solvation energies, and solvent forces utilizing the smooth Gaussian-based dielectric map functions and the quadratically smooth charge inverse-interpolation scheme described in the Methods section. This section makes use of a data-set of small molecules obtained from the Cambridge Structural Database (CSD),[32, 33] by searching for all molecules that possess the term "drug" or "activity" in the CSD text qualifier field. For each of these CSD structures, we only kept individual molecular fragments with more than six atoms, to exclude common fragments such as water, methanol, ammonium ions, etc. The largest molecule in the resulting data set has 196 atoms, and the average atom count is approximately 43 atoms (of which on average 21 are hydrogen atoms). These molecules were assigned atomic-charges using the Insight II interface to the CVF91[34] force field, resulting in 1558 neutral molecules and 418 ionic (charged) molecules. The precise distribution of molecules with a given ionic charge is given in Table I. This table also gives average solvation energies for molecules of each charge type. These are calculated using the standard molecular surface approach at a grid scale of six grids per Angstrom (gpa), and are quoted to illus-

TABLE I.
Distribution of Ionic Charge and Average Solvation Energies in the CSD Molecule Set.

Ionic Charge (e)	Number Molecules	Average Solvation Energy (kT)
−3	6	−771.4
−2	16	−385.7
−1	37	−151.3
0	1558	−25.2
1	340	−118.8
2	18	−336.4
3	1	−480.5

trate the range of solvation energies for our molecular data set. The energies in this and all subsequent tables are quoted in units of kT, where kT is the thermal energy computed at 298 K, such that 1 kT unit is equivalent to 2.478 kJ mol^{-1} (0.592 kcal mol^{-1}). The value of the permittivity at appropriate grid points is given by eq. (6). In this work the parameters of the underlying atom-centered Gaussian functions, are those obtained in our previous work to compute the volumes of small molecules.[20, 21] The Gaussian height parameter in (3) is $p_A = 2.70$, and the dimensionless scaling exponent in (3) is $\kappa = 2.3442$. From these parameters it is possible to compute the Gaussian density $\rho_{sum}(\mathbf{r})$, but it is still necessary to establish a value for the exponentiation constant A.

The primary motivation behind this work is to improve aspects of grid-based computational approaches to solving the PBe, with the emphasis on introducing the advantages of a smooth continuously differentiable function, as discussed in the Methods section. However, we wish to maintain a reasonable contact with solvation energies computed using the molecular surface, for reasons outlined in the Introduction. Our methodology is, therefore, to find optimal values for A by comparison between our new method and molecular surface calculations carried out under the same numerical conditions. The emphasis here is upon accuracy, so that for both sets of calculations we have adopted the same grid-charge distribution scheme, namely the quadratic inverse interpolation method described in Appendix B. In addition, we have chosen a discretization at 6 gpa in both cases, and the grid dimensions are determined to ensure a buffer region of high dielectric shown to be large enough that it does not effect the results. The boundary conditions for the solution of the PBe are set using the analytical coulombic potential. To quantify the variation of solvation energy with respect to grid orientation for 6 gpa calculations, we carried out molecular surface calculations for all molecules in our CSD subset in which the solute dielectric constant is set to unity and the solvent dielectric constant assigned the value 80.0. For each molecule we produced 50 random grid orientations by adopting an unbiased scheme using a quaternionic representation described by Vesely[35] based on a prescription given by Marsaglia.[36] We then examined the scatter by looking at the root-mean-square (rms) deviations in the solvation energies. We found that the mean deviation over the whole set of molecules was 0.11 kT, that 50% of the molecules had deviations of less than 0.007 kT, and that all molecules had less than 0.92 kT deviation. This is a very clear indication that 6 gpa is accurate enough for the purpose of parameterizing the value of the exponentiation constant A. The methodology adopted to find the optimal A is described in what follows. For a fixed value of A we carried out PB calculations utilizing the Gaussian dielectric function at 6 gpa and plotted the Gaussian against the molecular surface solvation energies for the whole set of molecules. For reasonable values of A the data fall on a straight line with very little scatter (see Fig. 3). It is clear that the optimal value of A should give a straight line with zero intercept and a unit slope. Our procedure is to adjust A to find a value that gives an intercept as close to zero and a slope as close to unity as possible. It is evident from the data in Figure 3 that the data points are clustered along the fitted line, and, as expected, that the clusters are related to ionic charge. Our strategy for finding the best A was adopted to ensure that the small number of highly charged molecules at the bottom left of the graph did not skew the results. We could have clearly adopted a strategy in which we sought a different A for each charge state. We felt, however, that there was a merit, in adopting a universal approach with a single value of A. The graph in Figure 3 shows our best fit of $A = 11.8$, which leads to an intercept of -0.024 kT and a slope of 0.999. The accuracy of the fit for such a wide range and large number of small molecules justifies our search for a universal "molecular" value of the A parameter. Although there is a single A parameter for all grid scales, there is not a single A parameter for arbitrary differences in dielectric values. We have obtained values of A for widely used differences in dielectric values, using the procedure just described, and these values of A are given in Table II.

We next consider a comparison of the positional and grid-scale dependencies in the calculation of

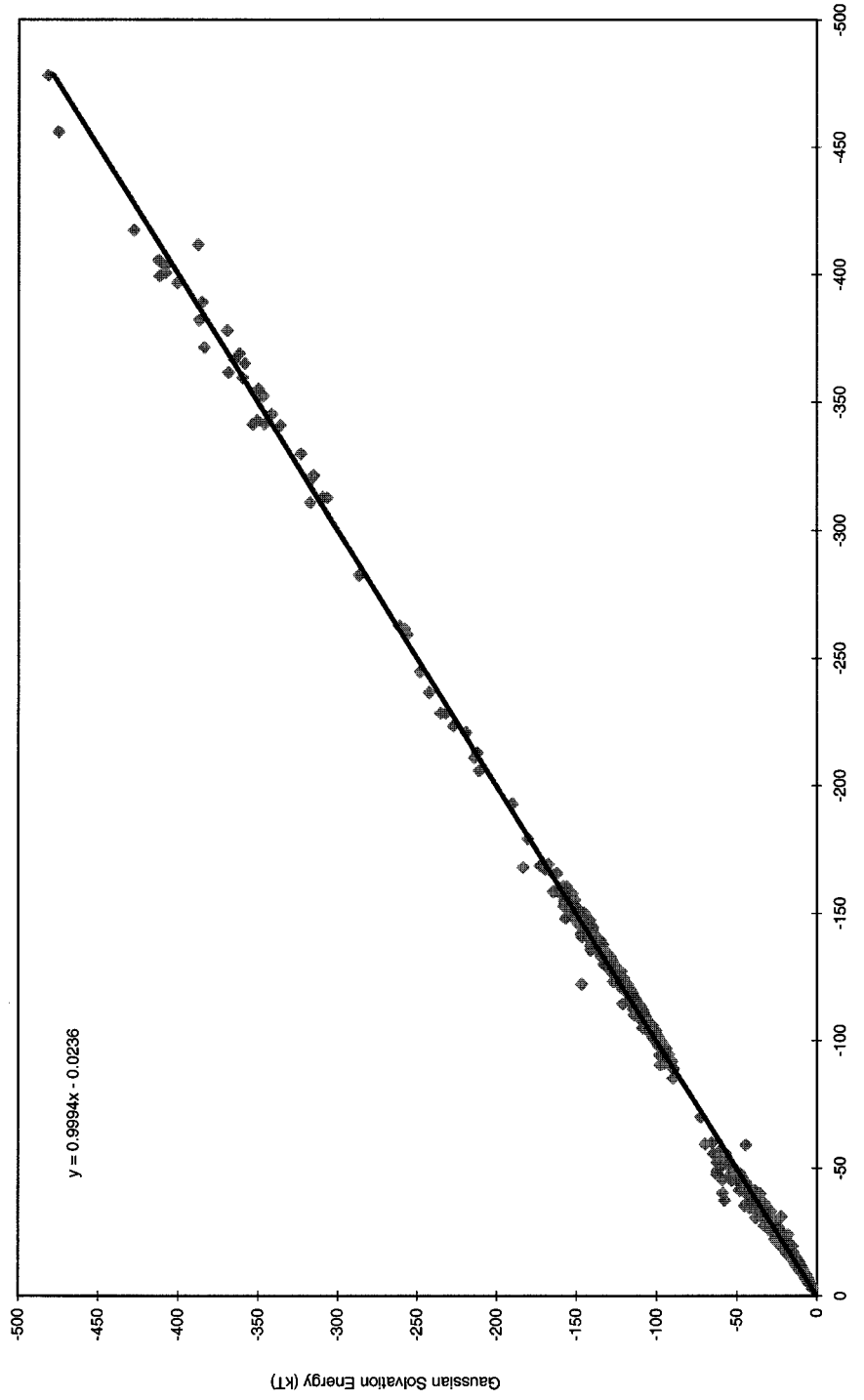

FIGURE 3. Plot of solvation energies for Gaussian vs. Molecular Surface methods for all molecules in the CSD data set (for clarity, ionic molecules with +3 charge have been excluded).

TABLE II.
Optimised *A* Values for Standard Dielectric Differences.

Inner Dielectric (ϵ^r_{solute})	Outer Dielectric ($\epsilon^r_{solvent}$)	*A*
1	80	11.8
2	80	9.8
4	80	8.0
10	80	6.0
20	80	4.8
2	1	2.2

PB molecular solvation energies using G(1/80) and MS(1/80) dielectric models. To give the reader an overview we have plotted in Figure 5 the translational dependencies of the solvation energy for a single molecule (CSD ref. code AMOADA) at different grid scales. The plots show the variation of solvation energy computed at 50 equally spaced intervals, as the molecule is moved along the *x* axis through one grid cell. It is clear that the MS calculations (broken lines) display a very spiky translational dependence, albeit one that is reduced as the grid scale increases. The Gaussian results, on the other hand, are smooth at all grid scales. The amplitude of the variation is always smaller for Gaussian compared to MS calculations, and the convergence to small amplitudes with respect to increasing grid scale is always quicker. It should be emphasised that both the G(1/80) and MS(1/80) calculations were conducted with quadratic charge interpolation. We found that the results for linear charge interpolation are similar except that the variations have larger amplitudes, and there are occasional cusps that arise from the nonsmooth behavior of linear interpolation when an atom-centered charge is positioned exactly at a grid point. Such behavior is eliminated by our quadratic scheme.

The behavior exhibited for the translational dependence in Figure 5 clearly demonstrates advantages in adopting Gaussian dielectric maps. This was investigated further by carrying out a detailed statistical analysis intended to accurately quantify orientational and grid-scale dependencies of molecular solvation energies. To this end we calculated solvation energies for 50 random orientations of each molecule in our subset of the CSD containing 1976 drug-like molecules. The calculations were performed using the G and MS methods at a range of grid scales up to an accuracy of 6 gpa. Each set of 50 orientations produces a mean solvation energy and a standard deviation. The statistics we describe refers to the distribution of these standard deviations (SDS). Hence, Table III shows the mean of these SDS, their standard deviations, their maximum and minimum values (i.e., the range), and the 99.5% quantile (i.e., the value of the SD below which lie 99.5% of the molecules) for the MS approach. It is readily apparent that the means and SDS decrease as grid scale increases, as expected. Table IV shows the corresponding data computed using the Gaussian method. Clearly, the Gaussian method has higher accuracy for any grid scale than the MS method, and the convergence with respect to grid scale is faster for the Gaussian method. Table V shows the statistics of grid scale dependence for the MS method formed by subtracting the mean solvation energy (from 50 orientations), at a fixed grid scale from the mean for the 6 gpa calculation (our most accurate calculations). The distributions show evidence for a bimodal distribution because of the different behavior for neutral and ionic molecules. The orientational behavior in solvation energy for ionic molecules is simple in that it is dominated by contributions from the presence of "full" charge(s), which polarize the solvent through the interaction of a spherically symmetric electric field. Polar neutral molecules, in contrast, have much stronger orientational dependence, which comes from the relative orientations of a dipolar electric field within an arbitrarily shaped dielectric cavity. It is obvious that the means and SDS in Table V rapidly decrease as the grid scale increases. Table VI shows the equivalent data for the Gaussian method, in which the accuracy is clearly improved compared to the MS.

An elegant summary of the statistical behavior of errors obtained for the CSD data set, using the Gaussian method, is shown graphically in Figure 4. The histograms represent expected errors in solvation energies for neutral molecules, arising from grid scale and positional dependencies. The smooth line represents the total expected error in PB solvation energies, at different grid spacings. This total error assumes that grid scale and positional errors are uncorrelated and is defined to be the norm of these two errors. The total error decreases smoothly in the range between 1 and 2 gpa from around 2% to approximately 0.5%. A similar analysis for charged molecules has total expected errors that are only roughly one-quarter of those obtained for neutral molecules. The errors shown in Figure 4 have been calculated using an interpolation method for averaging permittivities at neighboring grid points to permittivities at cell face centers. This method will be fully described in a forthcoming article.[37]

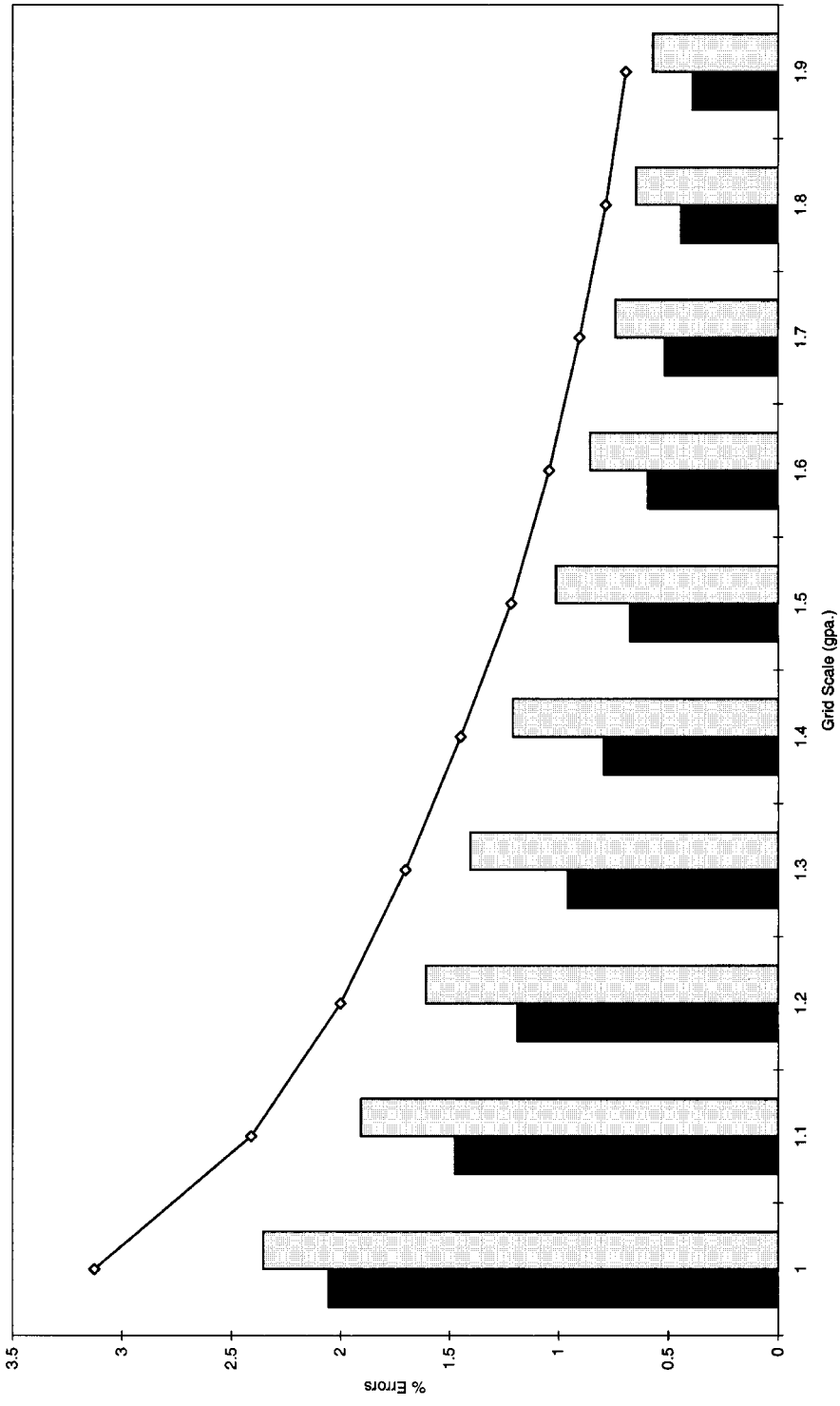

FIGURE 4. Expected errors at different grid scales in neutral small molecule solvation energies for the Gaussian method. The solid line represents the total error expected. The underlying bars represent the explicit grid scale (dark) and positional errors (light).

FIGURE 5. The dependence of E_{solv} on position with respect to the grid for the G (solid lines) and MS (dotted lines) permittivity functions. Fifty units along the abscissa represents molecular translation by one whole grid spacing. Results at 1 gpa and 2.0 gpa are shown in (a) and (b), respectively.

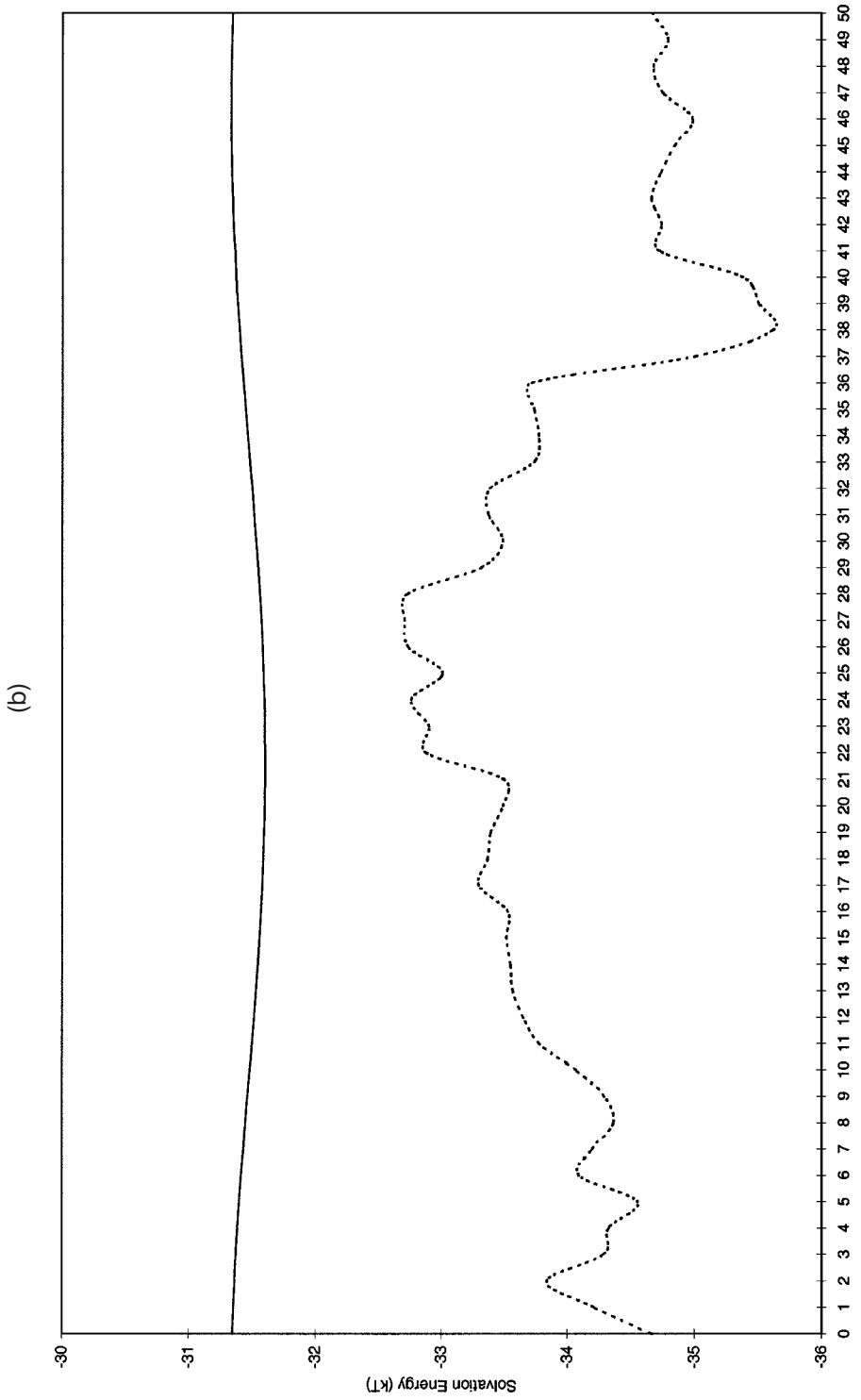

FIGURE 5. (Continued)

TABLE III.
Statistical Analysis of the Mean Variation of the Solvation Energy for Different Grid Orientations Using the Molecular Surface Permittivity Function.

Grid Scale (gpa)	Mean (kT)	SD (kT)	max (kT)	min (kT)	99.5% Quantile (kT)
1	1.626	0.921	9.151	0.000	6.376
2	0.795	0.452	3.489	0.108	2.590
3	0.277	0.195	3.798	0.037	1.053
4	0.198	0.137	2.310	0.023	0.854
5	0.127	0.102	1.107	0.012	0.636
6	0.112	0.106	0.917	0.009	0.633

TABLE V.
Statistical Analysis of Differences in Solvation Energies with Respect to a 6 gpa Reference for the CSD Molecule Set Using a Molecular Surface Permittivity Function.

Grid Scale (gpa)	Mean (kT)	SD (kT)	max (kT)	min (kT)	99.5% Quantile (kT)
1	6.356	5.347	29.247	−5.746	23.249
2	8.341	3.744	20.945	0.624	17.855
3	2.317	1.300	11.020	−1.262	7.049
4	1.297	0.881	4.335	−2.542	3.180
5	0.423	0.675	4.776	−2.646	3.329

BORN IONS

A simple picture of solvation is presented by the analytic Born ion model, in which a charge Q is placed at the center of a sphere of radius σ with a discontinuous dielectric boundary. We investigate the properties of our continuous dielectric model for single ions. In Figure 7 we show the values of solvation energy computed at 6 gpa using the G(1/80) model, multiplied by ion radius (σE_{solv}) for different values of the A parameter. It is clear from the expression for the Born ion solvation energy viz.;

$$\sigma E_{solv} = \frac{Q^2}{8\pi\epsilon_0}\left(\frac{1}{\epsilon^r_{solvent}} - \frac{1}{\epsilon^r_{solute}}\right) \tag{23}$$

and the straight lines of Figure 7, that our Gaussian dielectric model satisfies the same scaling as the analytical Born ion model. This is by virtue of the direct dependence of the Gaussian ρ^g_A on r_A/σ_A in eq. (1), which ensures simple scaling properties for the dielectric function. Most importantly, the graphs demonstrate that the absolute value of the solvation energy decreases with increasing value of the A parameter. This can be trivially deduced from the form of the permittivity function in eq. (6). For example, the half radius $r_{1/2}$ of the dielectric function in (6), i.e., the value of r, which is halfway between solute and solvent dielectric values, satisfies:

$$\left(\frac{r_{1/2}}{\sigma}\right)^2 = \frac{1}{\kappa}\ln\left(\frac{Ap}{\ln 2}\right) \tag{24}$$

and the slope at this position is:

$$\left.\frac{d\epsilon}{dr}\right|_{r_{1/2}} = \left(\epsilon^r_{solvent} - \epsilon^r_{solute}\right)\frac{\kappa r_{1/2}\ln 2}{2\sigma^2} \tag{25}$$

It follows that $r_{1/2}$ increases logarithmically with A, and that the slope increases linearly with $r_{1/2}$. Hence, as A becomes larger, the dielectric transition region increases in effective radius, but becomes narrower. The solvent polarization arises from the transition region, so the further out that lies, the smaller the interaction between the central charge and the polarization, and hence, the lower the solvation energy. The value of A, which reproduces the Born Ion model is $A = 16.6$, which is significantly larger than $A = 11.8$, which is the optimal value for

TABLE IV.
Statistical Analysis of the Mean Variation of the Solvation Energy for Different Grid Orientations Using the Gaussian-Based Permittivity Function.

Grid Scale (gpa)	Mean (kT)	SD (kT)	max (kT)	min (kT)	99.5% Quantile (kT)
1	1.010	0.586	4.586	0.136	3.754
2	0.175	0.087	0.628	0.025	0.507
3	0.054	0.024	0.184	0.007	0.152
4	0.026	0.012	0.119	0.002	0.074
5	0.016	0.008	0.070	0.002	0.050
6	0.011	0.006	0.053	0.001	0.036

TABLE VI.
Statistical Analysis of Differences in Solvation Energies with Respect to a 6 gpa Reference for the CSD Molecule Set Using a Gaussian Permittivity Function.

Grid Scale (gpa)	Mean (kT)	SD (kT)	max (kT)	min (kT)	99.5% Quantile (kT)
1	4.682	2.225	13.162	0.331	10.289
2	1.377	0.661	4.394	0.077	3.444
3	0.239	0.135	0.949	−0.033	0.679
4	0.073	0.043	0.077	−0.067	0.211
5	0.007	0.037	0.140	−0.020	0.070

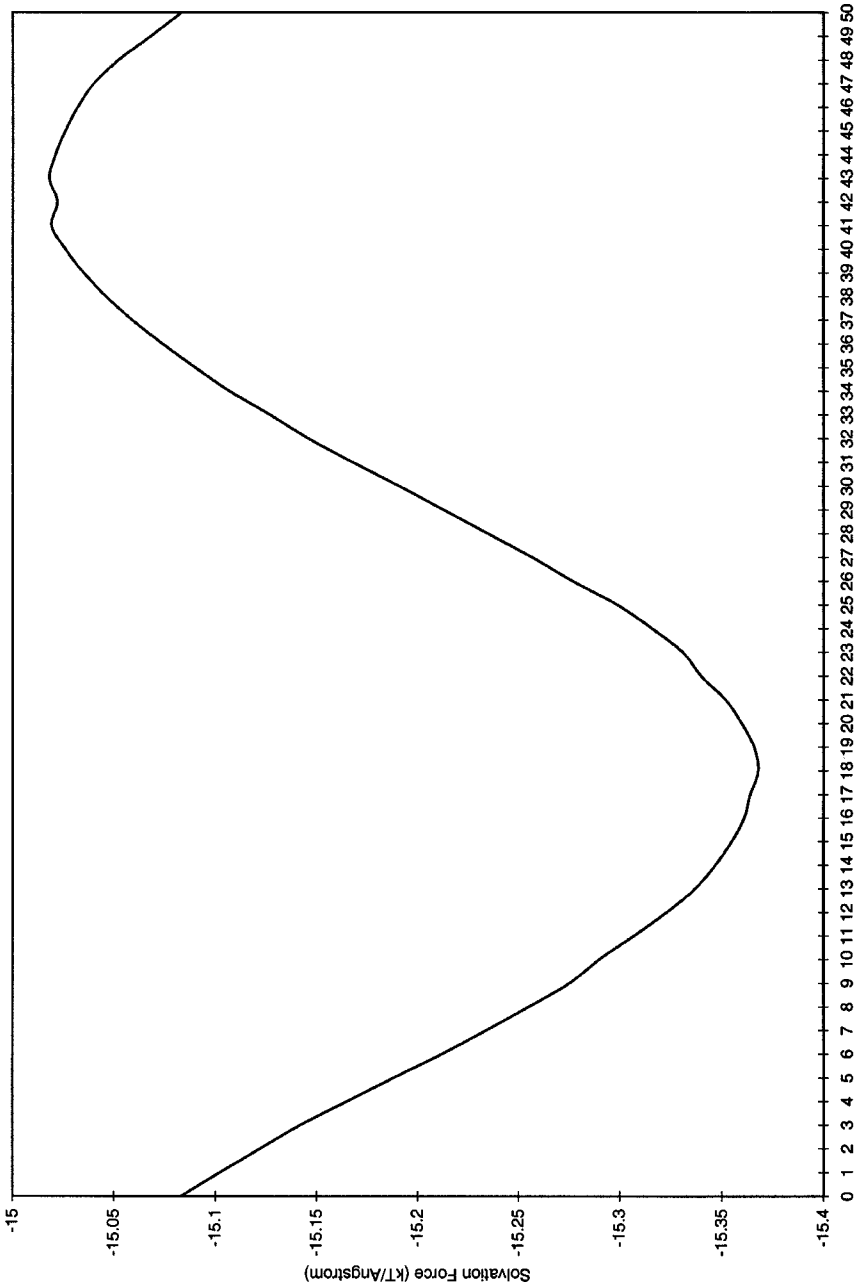

FIGURE 6. The dependence of a component of the solvation force on a single atom for the AMOADA molecule at 2 gpa for the G permittivity function. Fifty units along the abscissa represents molecular translation by one whole grid spacing.

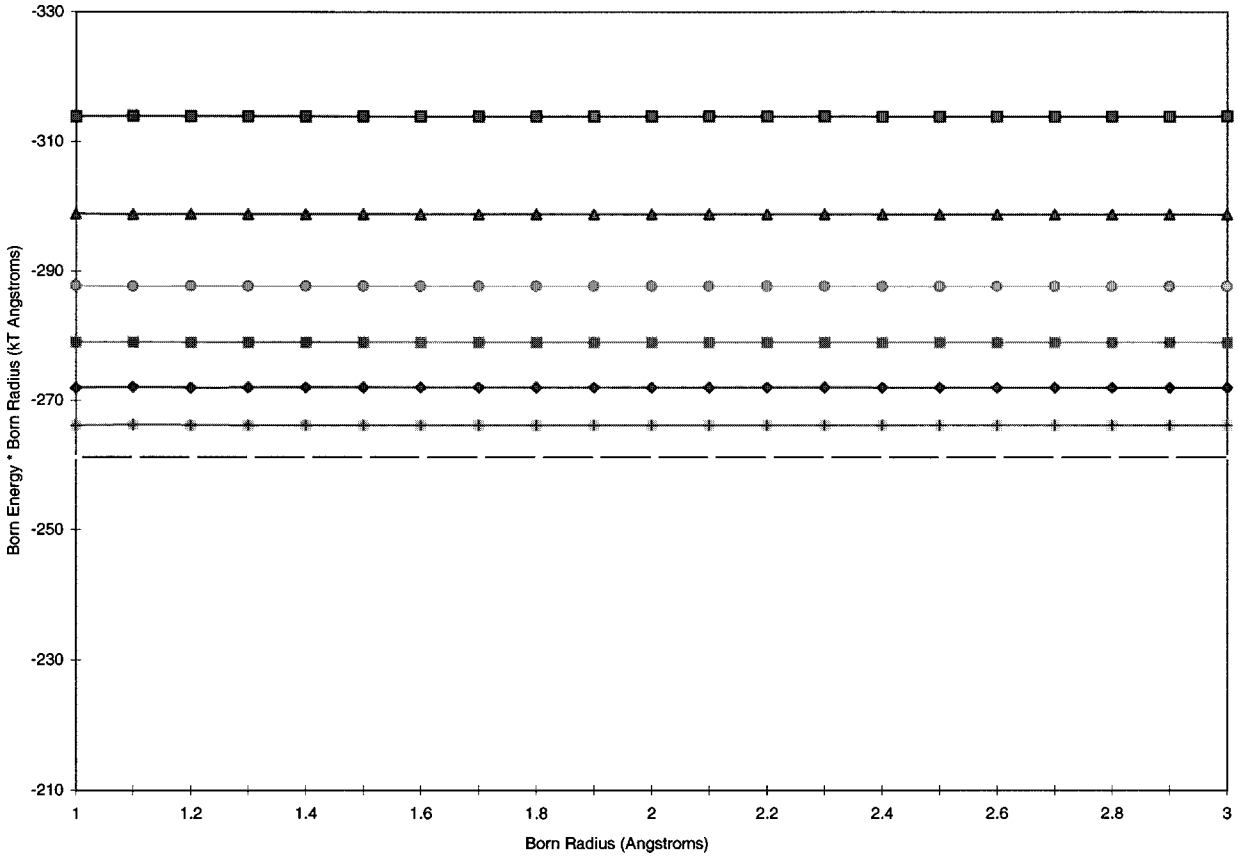

FIGURE 7. σE_{solv} plotted against σ for various A values using the Gaussian permittivity function. The lines from top to bottom represent $A = 10$ to 22 in steps of two units.

molecules. However, by uniformly increasing the radii of ions by 10% for $A = 11.8$ it is possible to reproduce exactly solvation energies computed using $A = 16.6$. Clearly, such uniform scaling would not be appropriate if the lines plotted for different A values in Figure 7 were other than straight. This scaling feature is very similar to that deduced by Honig et al.,[38] to reproduce experimental solvation enthalpies of multivalent atoms using the Born model. The Gaussian model solvation energies computed using $A = 16.6$ reproduce the analytical Born solutions very accurately.

It is likely that in molecules the use of $A = 11.8$ gives better answers because of the need to exclude water from fine-scale crenellations at the solute–solvent boundary arising from atomic overlap. Although smaller A contracts the position of the transition region with respect to atomic centers, it gives rise to a larger transition window, which acts to smooth out variations in the dielectric function, effectively excluding solvent from regions of high atomic overlap. It might be expected that molecular ions require an A value similar to Born ions (because the ionic charge is likely to be highly localized), but we do not find this in practice. The results described for molecular solvation energies confirm the suitability of a universal A value, for ions and neutral molecules.

SOLVENT FORCES

We now consider the calculation of the solvent forces using the Gaussian dielectric model, and eq. (22). Figure 6 is a plot of the translational variation of a typical force component on an atom of the molecule used for Figure 5 at 2 gpa. It can be seen that although there is variation in this force component, it is smooth, with a very small amplitude. In contrast, molecular surface approaches contain inherent force discontinuities. Im et al.[26] observed force discontinuities because of their linear charge interpolation onto the grid.

The implementation of the calculation of solvent forces can be trivially checked by comparing the analytical method to solvent forces obtained from numerical differentiation of the electrostatic solvation

energy. We have carried out such calculations (also referred to as the "virtual work method"[27]) using a steplength of 0.01 Å and analyzed results for all force components greater than 1 kT Å^{-1} for atoms of all 1976 molecules in the CSD data set. The mean difference between the numerical and analytical gradients for 84,581 data observations is 0.00 (zero) kT Å^{-1} to two decimal places at 2 and 4 gpa, and the standard deviations are 0.17 and 0.13 kT Å^{-1}, respectively. To investigate the grid stability we computed the total force on each atom for all molecules in the CSD data set, for 50 random orientations of each molecule. The means of the standard deviations at grid scales of 1.5, 2, and 4 gpa were 0.20, 0.10, and 0.01 kT Å^{-1}, respectively. Thus, the stability on the grid is excellent even at low grid scales, and the improvement as grid scales increase parallels that found for the solvation energy. Minimizing errors in solvation energies and their gradients is particularly important when optimising the geometry of flexible molecules, because the presence of spurious grid terms can cause optimizers to find the wrong geometries, or to be deflected from a smooth convergence to the optimal geometry. Similar situations occur in computing trajectories in Molecular or Brownian dynamics. The accuracy observed in the results we have described computing solvent forces are to be expected from the fact that we have introduced a smooth permittivity function that abolishes both the discontinuous dielectric boundaries and instabilities arising from the collapse of high dielectric regions as atoms are moved. The stability also arises from the quadratic charge interpolation scheme that gives continuous charge derivatives as atoms are moved. We have further tested our Gaussian dielectric model by combining the resulting solvent forces with the CLEAN[39] force field, so that energy minimizations can be carried out with the effects of solvent included.

As an illustrative example, we carried out calculations on blocked alanine (*N*-acetyl-*N*-methylalanineamide). Figures 8 and 9 show the *vacuo* and solvated energy surfaces in peptide phi–psi space, for blocked alanine. The latter energy surface is obtained by including the PB solvation energy computed at 2 gpa. At this grid scale the energy surface is perfectly smooth. At lower grid scales a degree of coarseness was found in the energy surfaces, but the position in phi–psi space of the minimum in Figure 9 are hardly affected. The change in the energy surface upon solvation largely arises from the preferential solvation of approximately parallel aligned amide (peptide) dipoles, relative to the antiparallel arrangement found in the gas phase. The

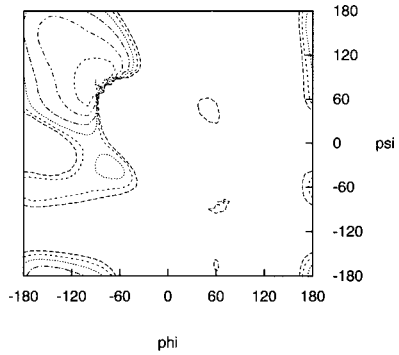

FIGURE 8. Gas-phase energy E_{gas} (in kT units) plotted as a function of the (ϕ,ψ) torsional angles for blocked alanine.

global minimum in the gas phase is also stabilized by an internal hydrogen bond, a feature absent in the structures favored when the effects of solvent are accounted for. These features of blocked alanine phi–psi energy surfaces are well known, and despite the approximate nature of the CLEAN force field, the *vacuo* energy surface compares well with those obtained from accurate quantum methods.[40] The change in energy surface when the effects of solvent are included, are consistent with experimental observations of phi–psi dihedral angles observed for alanine residues in peptides and proteins,[40, 41] and the dominant conformers observed in solution from measurements of NH—C$^{\alpha}$H vicinal coupling constants.[42]

We performed energy minimizations for blocked alanine, starting at arbitrary points on the solvated phi–psi energy surface. We found smooth convergence to minima found in Figure 9 at 2 and 3 gpa. At 1 gpa, we occasionally observed less optimal behaviors. The most pernicious of such is convergence to false minima. More prevalent is convergence to the

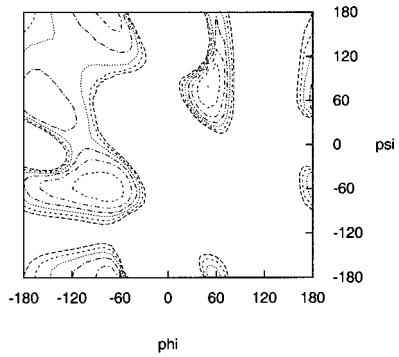

FIGURE 9. Solvation energy E_{solv} (in kT units) plotted as a function of the (ϕ,ψ) torsional angles for blocked alanine.

correct structure, but to a significantly lower energy (by ≈7%) than we expect from the previous error analysis. This arises because, in addition to minimizing the interatom and atomic–solvent energies, we are also minimizing the artifactual "grid energy," i.e., we are finding the energy corresponding to the "best" orientation on the grid. We are investigating methods of ameliorating such behavior.

APPLICATIONS TO PROTEINS

Although external potentials are similar, visualization reveals that using the Gaussian approach there is a greater degree of heterogeneity in the description of the dielectric of the protein interior than obtained using the dual-valued molecule surface method. We were, therefore, concerned as to the utility of our method for protein electrostatics. Specifically, would the method exclude water sufficiently from the interior of proteins? Because most protein biochemistry occurs at the surface of proteins, not inside, does it matter? Three common uses of the PBe were considered: the computation of protein desolvation energies, the estimation of pKa shifts of ionizable residues, and the binding of small ligands to active sites.

The atomic coordinates of the protein structures used in this section are taken from the PDB.[43] Hydrogen atoms were added to these structures using a simple dictionary facility, followed by an energy minimization in which only the hydrogen atoms are allowed to move. The potential function used for the minimizations and the charge distributions used for subsequent electrostatic computations are taken from CHARMM Version 22.[44]

Protein Residue Derivation Energies

A quantitative measure of the removal of water from protein crevices and interiors is obtained by calculating the desolvation of each residue. There can be a substantial penalty in solvation energy incurred when a polar or charged residue is buried within a protein. Conversely, residues close to the surface of a protein may be accessible to solvent, but still partially desolvated. An accurate account of residue desolvation energies is of considerable importance in the computation of pKas and binding energies. If the Gaussian model fails to exclude water, then the desolvation penalties will be much lower than with the molecular surface model. Figure 10 plots Gaussian against Molecular Surface desolvation energies for Lysozyme, computed using a protein dielectric value (ϵ^r_{solute}) of 2. It is clear from this graph that the two methods give strongly correlated desolvation penalties, although those computed using the Gaussian-based dielectric function are systematically smaller than those obtained using the Molecular Surface. We have also compared the MS(4/80) desolvation penalties with G(2/80) in Figure 11. It is immediately obvious from this plot that the desolvation energies computed in this way are approximately equal.

This was a suprise. Gilson predicted[45, 46] that, due to internal carbonyl motion, proteins might rigorously have a dielectric of around 4. In addition, some workers have found that such an assignment improves the accuracy of many physical predictions for proteins. We discuss this further in what follows.

Protein pKas

Having observed the desolvation behavior of the Gaussian model, the question remains as to the effect of this in predicting physical properties. One such is the pKa of ionizable groups, predominantly aspartic acid (ASP), glutamic acid (GLU), lysine (LYS), arginine (ARG), and histidine (HIS). It is known that shifts in pKas can result from burial in the protein interior and from the interaction with other charged and polar groups within the protein, both of which are quantifiable by the PBe. Several groups have addressed this problem with varying degrees of success.[47–51] Gilson has shown[46, 52] that the "Null" hypothesis in which pKas assume the value of model compounds (and are thus "Null" shifted) can perform better than using the PBe. He also observed that if the protein dielectric constant is set to 20 rather than 2 or 4, for which there is theoretical justification,[3, 45] better correlation to experiment was found. Gunner[53] has suggested that the problem lies in the assignment of proton positions, given that these can be relatively mobile. A detailed treatment of proton positions greatly complicates the calculation, but makes more physical sense than using a dielectric of 20 throughout a protein. Seen in this light, our observation that residues are not as desolvated using the Gaussian model, might actually be an advantage. We retain the fundamental low dielectric of the protein body but allow for partial ingress of water disallowed by the molecular surface scheme.

We have written adjunct programs to ZAP to explore pKa shifts. The calculation is based on a two-state all-atom representation of the ionizable residue. Titration curves for each ionizable residues are obtained using a Monte Carlo algorithm[54] to calculate a statistical mechanical average residue-

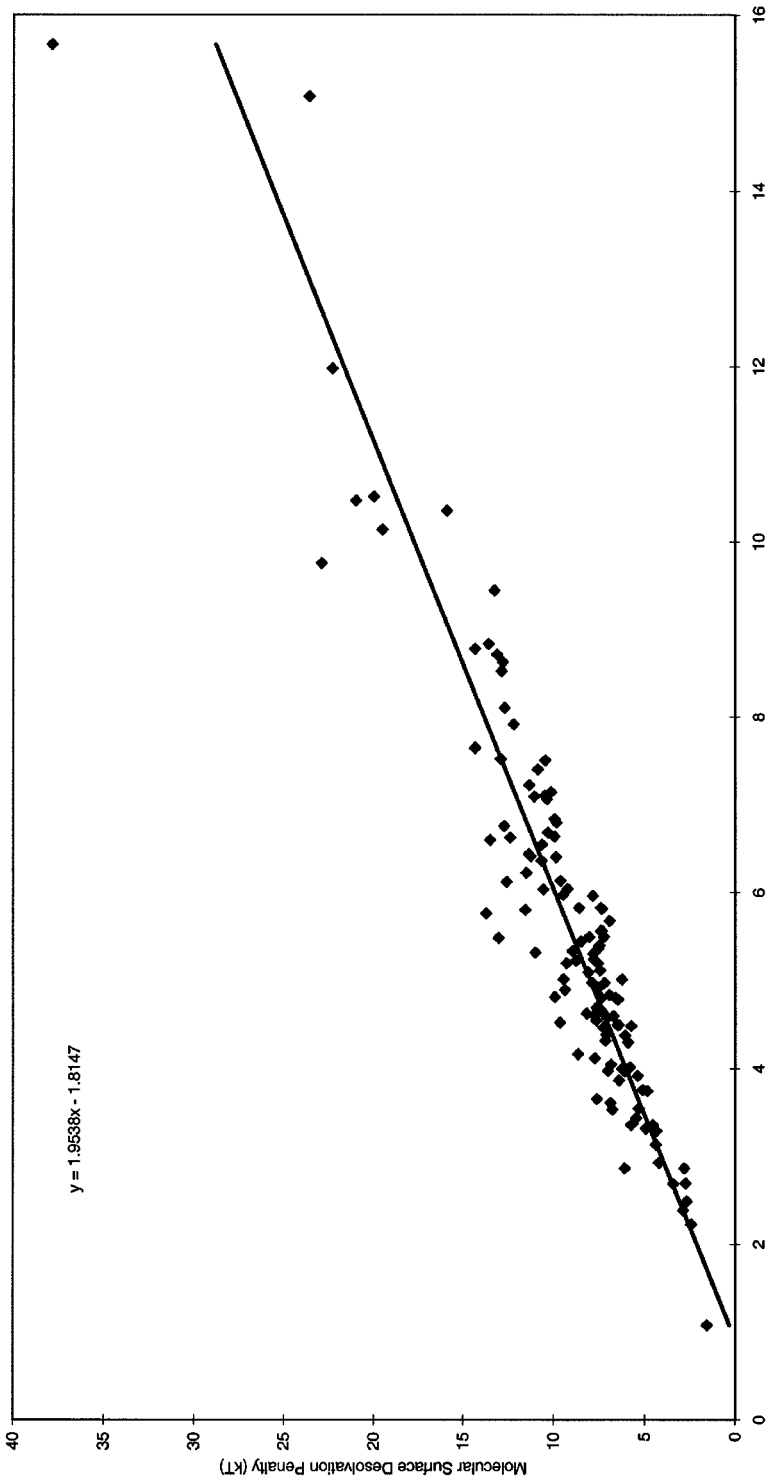

FIGURE 10. Lysozyme residue desolvation penalties for G(2/80) and MS(2/80) models.

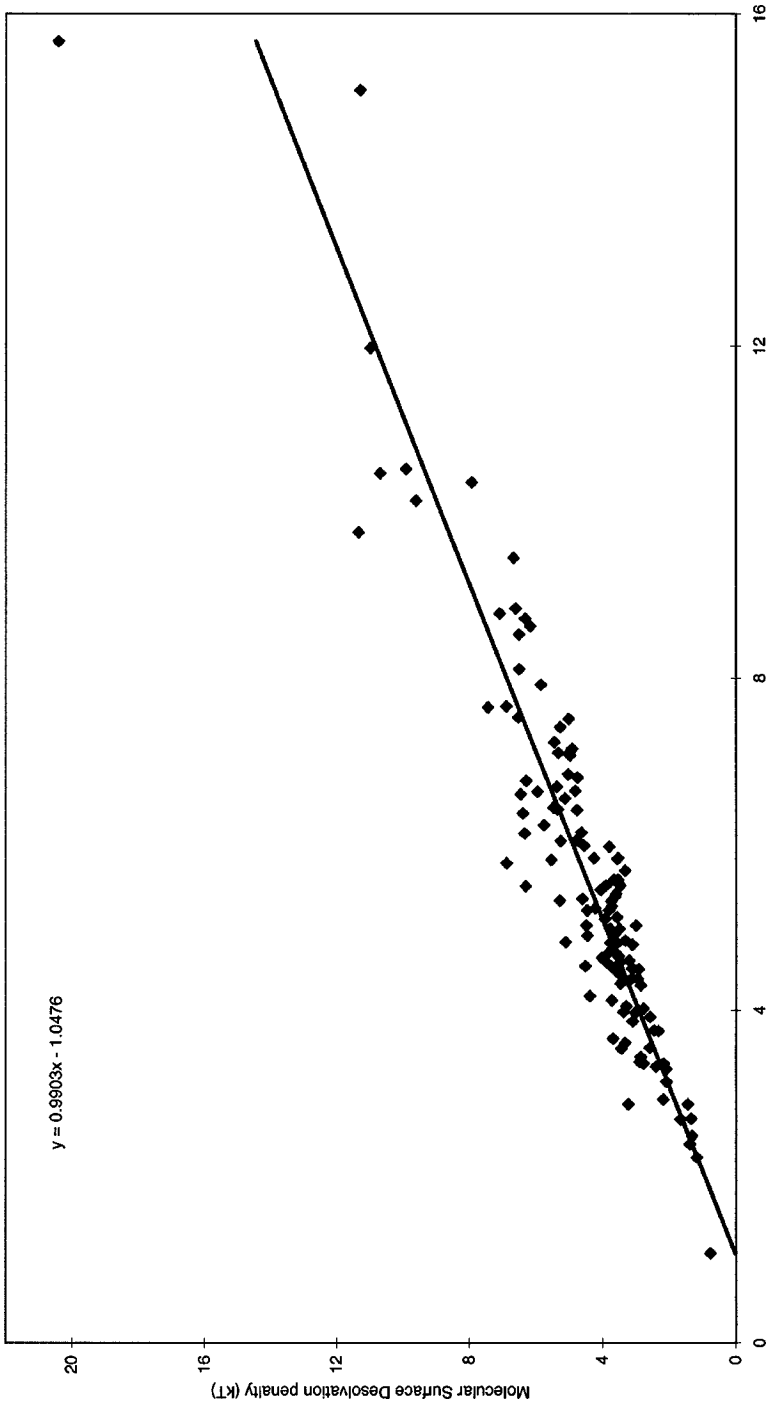

FIGURE 11. Lysozyme residue desolvation penalties for G(2/80) and MS(4/80) models.

occupancy from an ensemble of protonation states. Differences in free energy between protonation states are assumed to arise from a linear response of the system to ionization, and as such are computable from a symmetric matrix of interaction free energies between ionizable residues. This matrix is computed by focussing[2] onto ionizable residues to calculate desolvation penalties and interactions to other groups. The Gaussian model has efficiency advantages over previous methods for these procedures, and the time required is much less than previously reported. Details will be published elsewhere.

Tables VII and VIII give pKas for Hen Egg White Lysozyme (HEWL) and Turkey Ovomucoid Third Domain (OMTKY3) calculated using G and MS models, based on both 2/80 and 4/80 dielectric values. Isolated amino acids in solution were assumed to have the values; ASP 3.9, Glu 4.3, His 6.5, and Lys 10.5. For HEWL and OMTKY3 crystal structures are used, taken from the files 2lzt and 1ppf, respectively. The proton placement and ionization state sampling procedures are identical for all calculations. The results show that the calculated pKas in the Gaussian model are reasonably consistent with experiment. pKas calculated using the G(2/80) model are very similar to those calculated with MS(4/80). This same trend was noted for the calculation of protein desolvation energies, and discussed in the previous section. There are small changes in computed pKas between the G(2/80) and G(4/80) models, in contrast to the significant changes observed between the MS(2/80) and MS(4/80) models. In fact, the MS(2/80) model provides a very poor description of pKa shifts, probably because of large errors in describing desolvation energies. It is important to emphasize that the pKa calculations carried out here lack the sophistication of those in which factors such as protein conformational flexibility are taken into account.[53] Our purpose was primarily to demonstrate that the Gaussian model reproduced pKa shifts and to compare such predictions with those obtained using the molecular surface model. For this reason it was vital to use calculations carried out using identical methodology.

TABLE VII.
Analysis of Calculated pKa Values for HEWL.

Residue	Expt[a]	G(2/80)	MS(2/80)	G(4/80)	MS(4/80)
LYS 1	10.6	9.1	7.9	9.5	8.9
GLU 7	2.6	2.6	2.8	2.6	2.6
LYS 13	10.3	10.0	10.0	10.0	10.1
HIS 15	5.8	5.1	1.9	5.4	4.2
ASP 18	2.7	2.2	2.1	2.4	2.1
LYS 33	10.4	9.8	9.1	9.9	9.6
GLU 35	6.1	5.5	8.1	4.7	5.9
ASP 48	1.6	1.1	0.9	1.6	1.6
ASP 52	3.6	3.9	5.2	3.5	4.2
ASP 66	2.0	2.5	7.3	2.9	4.7
ASP 87	3.4	2.5	4.6	2.4	3.1
LYS 96	10.7	10.2	8.2	10.2	9.2
LYS 97	10.1	10.5	10.2	10.4	10.3
ASP 101	4.1	3.2	5.7	3.1	4.3
LYS 116	10.2	9.6	8.1	9.8	9.1
ASP 119	2.5	3.0	3.8	2.7	3.1

[a] Taken from tabulations in ref. 53.

TABLE VIII.
Analysis of Calculated pKa Values of OMTKY3.

Residue	Expt[a]	G(2/80)	MS(2/80)	G(4/80)	MS(4/80)
ASP 7	2.7	2.4	2.0	2.7	2.6
GLU 10	4.1	3.9	4.0	2.7	2.6
LYS 13	n/a	10.7	9.3	10.8	10.1
GLU 19	3.2	1.9	2.9	2.6	3.1
ASP 27	2.3	1.2	2.8	2.8	3.1
LYS 29	n/a	10.8	11.1	11.0	11.0
LYS 34	n/a	10.2	8.4	10.3	9.5
GLU 43	4.8	4.2	4.4	4.2	4.3
HIS 52	n/a	5.3	4.5	5.8	5.5
LYS 55	n/a	10.3	9.5	10.3	9.9

[a] Taken from tabulations in ref. 71.

We are confident from our investigations that the Gaussian dielectric model is useful for pKa calculations. A more advanced pKa algorithm would require a number of improvements, such as an extended description of the ionizable states of residues, the use of multiple solution-like protein conformers, better placement of hydroxyl protons, inclusion of salt effects, and a special description of salt bridges. For such sophistication to improve results it is necessary to have a dielectric model with low grid errors that leads to efficient computation. The Gaussian model possesses these features.

Binding Energies

The prediction of the energy of interaction of ligands and proteins is a hard problem because so many phenomena are involved that are difficult to quantify: the hydrophobic effect, bound waters, bound ions, entropy of binding, vibrational entropy, conformational entropy of the ligand, side-chain entropy of the protein, large-scale protein motion,

charge polarization, charge ionization (pKa shift in the active site), protein and ligand tautomerism, and hydrogen bonding, to list a few. Nonetheless, the need to understand binding as an elementary biological event, and the practical importance for the pharmaceutical industry in predicting affinities of potentially therapeutic molecules has inspired much research. Because PBe electrostatics captures much of the continuum behavior of water, such as solvation and screening stored quantify important elements of the binding event, and indeed, there have been some studies indicating its utility.[55–57]

The most noticeable result of PB energies of binding is that they are seldom favorable. It is a common misconception that opposite charges must attract. In water, the desolvation penalty of removing water from around charges often outweighs the charge–charge interaction. This applies to charged moieties such as hydrogen-bond donors and acceptors as much to fully ionized species, and as such, implies that hydrogen bonds made within a molecular complex are only stabilizing relative to configurations that leave such bonds unmade. We hoped similar behavior would be observed from the Gaussian model. We, therefore, implemented a standard thermodynamic cycle[58] to describe the change in total electrostatic energy when two molecules form a complex. The method permits an interpretation of binding in terms of the balance between the change in solvation energy from the interacting molecules, and the solvent-screened coulombic interaction energy.

There are a couple of technical difficulties in using the PBe for binding energy calculations. Proteins are large, and so grids that enclose them and still have a reasonable gridspacing may contain millions of points. Typical workstations may not have sufficient memory for such calculations which are, in any case, inordinately slow. Secondly, as described earlier, small movements of the ligand can instigate large changes in molecular surface (see Fig. 1). This corresponds to a water molecule being replaced from an active site by a ligand, which may cause a sudden change in binding energy. It is unlikely that the physics of water removal is so abrupt. Taken together, the size and stability issue have restricted the widespread investigation of the PBe and binding affinities.

The Gaussian approach improves matters. Water ejection becomes gradual as the ligand moves into the pocket, and calculated binding energies reflect this. An example is shown in Figure 12. This plots the variation in the electrostatic component of the binding energy of Rat-trypsin/Bovine Pancreatic Trypsin Inhibitor (R-Tp/BPTI, 3tgi[59]), as BPTI is translated from the experimentally observed position in the complex, in a direction approximately normal to the main surface–surface interaction. Although arbitrary, the identical trajectory is used for all computations. Figure 12 presents data computed using G(2/80), MS(2/80), and MS(4/80) dielectric models. The G(2/80) and MS(4/80) models are broadly comparable, whereas the MS(2/80) model predicts a much less favorable binding energy at the experimental separation, and the binding curve only begins to resemble the other models at separations of approximately 10 Å. The fundamental difference between the Gaussian and molecular surface binding descriptions is clearly revealed by considering the variation in the binding energy at short range. The Gaussian binding curve has a minimum at approximately 1.5 Å, whereas the molecular surface curve has no minimum, exhibits a large amount of noise due to positional instabilities, and possesses a sharp change in the binding energy in the region between 2 and 3 Å from the experimental orientation.

The total binding energy requires an estimate of the free energy associated with nonpolar interactions (ΔG^{np}). Viewing the process as the association of two nonpolar surfaces, ΔG^{np} can be approximated using:

$$\Delta G^{np} = \gamma \Delta A \tag{26}$$

where ΔA is the accessible surface area buried by the complex. γ is an interfacial surface-free energy obtained from partition coefficients of nonpolar solutes transferred from a low-dielectric solvent to water. The free energy in (26) is computed using $\gamma = 0.042\ kT$ (0.025 kcal mol^{-1})[60, 61] and combined with the electrostatic component, to obtain curves of the total binding energy, plotted in Figure 13. There is a broad minimum in the total binding energy using the combined area and G(2/80) positioned at approximately 0.75 Å and the penalty with respect to the experimentally observed minimum is only 1 kT. The magnitude of the binding energy is close to $-50\ kT$, compared to an experimental value of approximately $-23\ kT$, estimated from the reported dissociation constant.[59] This suggests that the unfavorable entropies associated with reduction in conformational, rotational, and translational degrees of freedom, account for a free energy of approximately 25 kT. The MS(4/80) model, when combined with the area free energy term, predicts a stable complex, with the minimum value in the binding energy similar to the G(2/80) model.

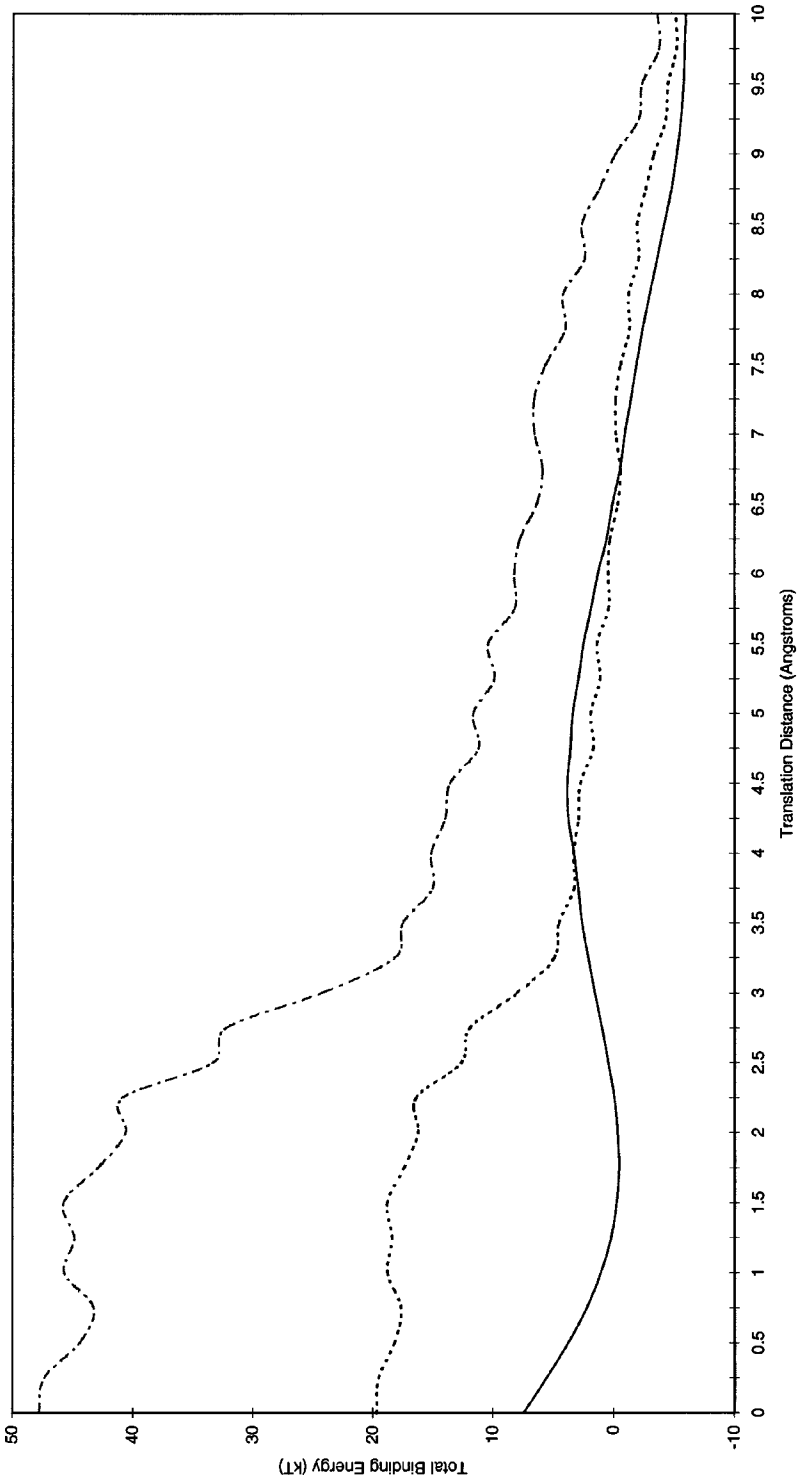

FIGURE 12. Translational variation in the electrostatic component of binding for R-Tp/BPTI using different dielectric models. Solid line is G(2/80), dotted line is MS(4/80), and dashed line is MS(2/80).

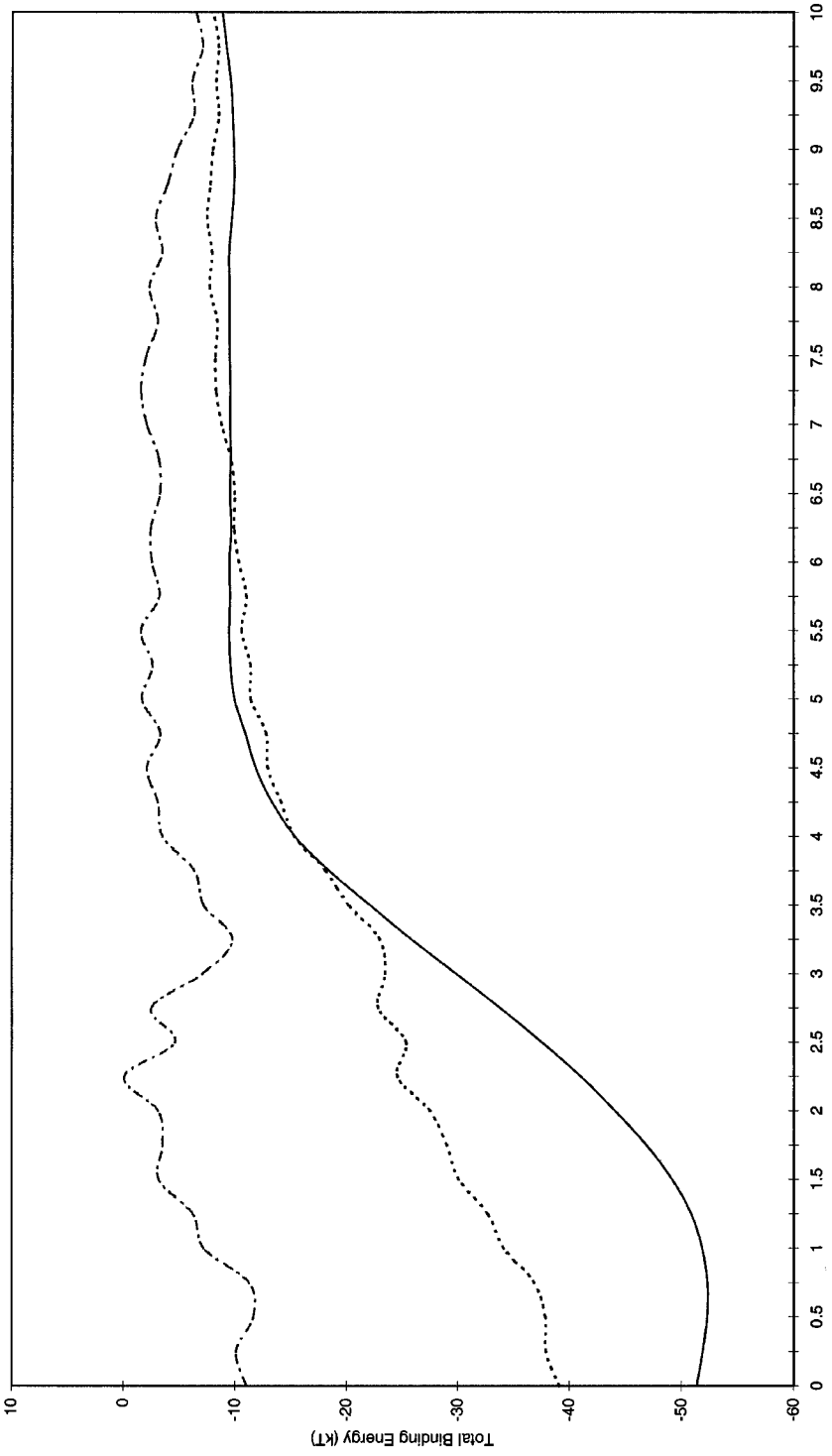

FIGURE 13. Translational variation in the total binding energy for R-Tp/BPTI using different dielectric models. Solid line is G(2/80), dotted line is MS(4/80), and dashed line is MS(2/80).

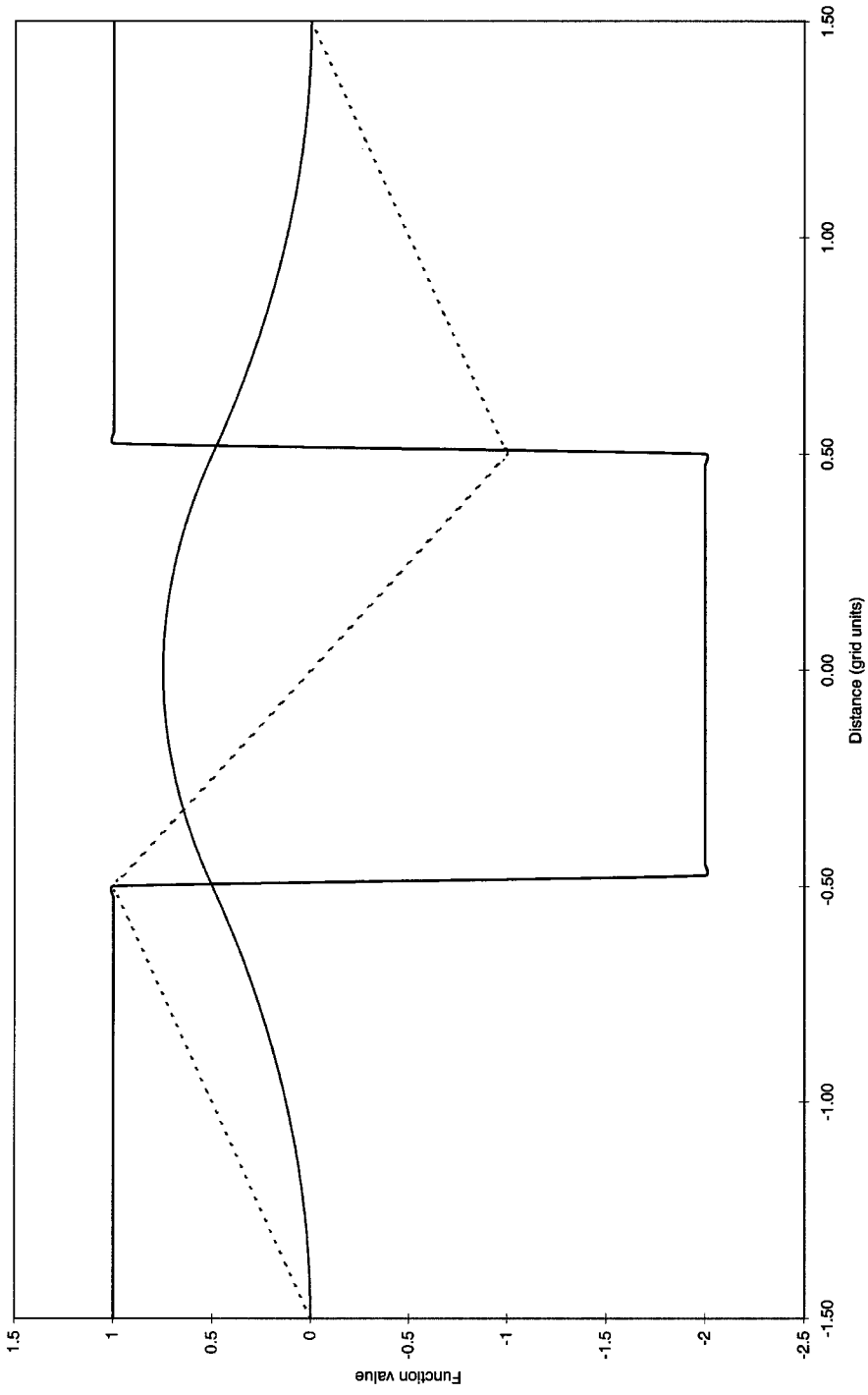

FIGURE 14. A Quadratic basis spline (smooth line) showing the behavior as a function of position. The first gradient (pecked line) is continuous but nonsmooth. The second gradient (solid line) is discontinuous.

TABLE IX.
Calculation of the Electrostatic Component of the Binding Energy Using Different Dielectric Schemes.

	G(2/80)			MS(2/80)			MS(4/80)		
Complex	T	D	C	T	D	C	T	D	C
1aaq	33.5	48.6	−15.1	119.1	134.2	−15.1	55.5	63.0	−7.5
1abe	15.6	42.9	−27.2	37.5	64.7	−27.2	17.0	30.6	−13.6
1acj	8.6	11.0	−2.4	34.7	37.2	−2.4	15.5	16.7	−1.3
1aha	4.9	15.8	−10.9	15.6	26.4	−10.9	7.2	12.7	−5.4
1apt	44.0	67.2	−23.3	122.4	145.7	−23.3	55.0	66.7	−11.7
1cbs	10.2	19.3	−9.1	42.2	51.4	−9.1	19.8	24.3	−4.5
1cbx	36.5	40.2	−3.7	64.1	67.8	−3.7	30.4	32.2	−1.9
1coy	8.1	11.6	−3.5	40.6	44.0	−3.5	18.8	20.8	−2.0
1cps	27.5	81.7	−54.2	79.2	133.4	−54.2	38.7	65.7	−27.1
1glp	7.6	29.3	−21.7	23.2	44.9	−21.7	10.6	14.2	−10.8
1hri	6.1	7.3	−1.2	26.6	27.8	−1.2	12.0	12.5	−0.5
1ida	28.7	42.2	−13.5	86.2	99.7	−13.5	39.8	46.4	−6.6
1lah	18.4	42.7	−24.4	31.6	55.9	−24.4	14.1	26.4	−12.3
1lmo	5.4	19.0	−13.6	17.9	31.5	−13.6	9.0	15.8	−6.7
1nco	11.9	22.0	−10.1	34.7	44.8	−10.1	16.6	21.5	−4.9
1slt	12.4	16.7	−4.3	26.4	30.7	−4.3	12.7	14.9	−2.1
1xid	42.2	63.2	−20.9	199.3	220.3	−20.9	85.3	95.7	−10.5

The issue of grid size can be resolved by the technique of grid focussing.[2] One starts by solving the PBe on a coarse grid that encloses the proteins and then uses this grid to approximate boundary conditions on a finer grid that encloses the active site but not the whole protein. Although this is a standard method, there has been no rigorous analysis of the errors that arise from the approximation of boundary potentials by this procedure. Boundary errors can be large if the embedded grid has a boundary that falls on either an atomic charge or crosses the dielectric boundary, the latter being inevitable if the grid enclosed is an active site. Such errors are formally identical to new source terms being added at each boundary grid point. The influence of such error charges can be reduced by enlarging the embedded grid, thus pushing them away from the center of interest. Potentials at the dielectric boundary vary more smoothly using the Gaussian model and the MS and, as a consequence, interpolation between grids of different scale is much more accurate. As such, the procedure for focussing between the Gaussian derived potential maps is more robust, and allows one to exactly match the area of interest and therefore are much smaller. A thorough analysis of focussing error and its application to the binding energy problem will appear in a future article. We have calculated the electrostatic component of the binding energies for a series of protein–ligand systems using both the Gaussian and Molecular surface dielectric schemes, and present the data in Table IX. The key features of this comparative data resemble those observed in the previous sections concerned with desolvation energies and pKas. That is, binding energies computed using G(2/80) are much smaller than the corresponding MS(2/80) data, but broadly resemble those computed using MS (4/80). However, in all cases this component of the binding energy is positive, although the penalties are generally the smallest for the G(2/80) models. The observation that electrostatic interactions tend to oppose binding has been found in previous applications of continuum solvent models. The reason for the difference in binding energies between the two approaches using $\epsilon^{r}_{solute} = 2$, is that for the Gaussian scheme, regions between the protein and ligand where a discrete water molecule cannot penetrate, are described by a continuous range of dielectric values higher than those found in the molecular interior. The consequences for computational speed of focussing using the Gaussian method are illustrated in Table X.

The relation of our new description of the binding process to experiment has also been investigated. The G(2/80) model combined with estimates of nonpolar interactions plus entropy contributions arising from rigid-body motion and internal rotations, has been used to predict experimentally

TABLE X.
Cpu. Timings for the Electrostatic Component of the Binding Energy Using the Gaussian Dielectric Model.

Complex	N Atoms (Protein)	N Atoms (Ligand)	cpu.[a] (s)	cpu.[b,c] (s)
1aaq	3156	91	3.1	34.6
1abe	4754	20	1.0	4.8
1acj	8409	30	1.7	8.7
1aha	3942	15	0.9	7.5
1apt	4603	82	2.5	26.8
1cbs	2238	49	1.9	16.9
1cbx	4846	27	1.4	9.2
1coy	7696	49	2.0	12.0
1cps	4848	34	1.3	7.3
1glp	3355	40	1.5	11.9
1hri	12591	48	3.2	22.8
1ida	3104	103	2.9	28.9
1lah	3719	20	1.0	5.6
1lmo	1978	57	1.6	13.6
1nco	3050	82	2.5	29.3
1slt	2039	51	1.3	9.6
1xid	6103	20	1.3	6.7

[a] 2 gpa.
[b] 4 gpa.
[c] cpu. times obtained using SGI R12K 300MHz (SPECfp95 = 28.0).

obtained dissociation constants of weakly binding ligands.[62] From a set of ligands that have been screened for binding to FKBP by NMR,[63] 47 were chosen, of which 27 have dissociation constants less than 5 mM, and thus classed as weak binders. Calculation using the augmented G(2/80) model correctly predicted 24 out of the 27 weak binders (three false negatives), and correctly classified 14 out of the 20 nonbinders (six false positives). A similar set of predictions was obtained for ligands screened for binding to a 24 kD fragment DNA Gyrase.[64]

COMPUTATIONAL PERFORMANCE

The calculations described have all been performed with the code ZAP. The adoption of a Gaussian dielectric function is well suited to optimizing the performance of grid-based PB calculations. We highlight key aspects of the current performance of ZAP by considering conjugate-gradient energy minimizations for a few protein systems. For these calculations the ZAP computation of PB forces has been integrated with the optimizer and protein molecular mechanics functionality of TINKER.[65] The CHARMM Version 22[44] force-field is used to represent the intramolecular empirical energy, and

TABLE XI.
Cpu. Timings for Single Gas Phase and PB Energy and Gradient Evaluations for a Few Protein Systems.

PDB Code	N Atoms	Gas Phase cpu.[a] (s)	PB (2 gpa) cpu.[b,c] (s)
2int (frag)	238	0.1	0.6
1crn	642	0.3	2.0
2lzt	1961	2.6	8.5
3app	4552	14.2	22.4

[a] Charmm22 energy and gradient.
[b] PB energy and gradient.
[c] cpu. times obtained using SGI R12K 300MHz (SPECfp95 = 28.0).

the PB computations are performed using a grid spacing of 2 gpa. Table XI gives cpu timings for the evaluation of the energy and gradient terms used in optimization. The timings indicate that the PB method scales approximately linearly with respect to system size, and for larger systems the PB part of the calculation is similar in cpu. requirement to that of the gas phase. These timings represent approximate benchmarks for the performance of ZAP, and indicate the feasibility of incorporating PB terms into energy minimization schemes to optimize protein structures, and refinement procedures of X-ray or NMR data.[66] However we anticipate improvements in the performance of ZAP, by ameliorating errors produced by coarser grids.

Discussion and Conclusion

This work describes in detail the construction of a continuously varying dielectric (permittivity) function, and the picture of solvation that emerges from using it to solve the PBe. For small molecules, solvation energies computed using our continuous model are nearly identical to those obtained from using a discrete dielectric boundary based on the molecular surface (MS). This agreement is by design, and was considered vital given the success of the MS model to predict experimental solvation energies of small molecules. For proteins the continuously varying dielectric function behaves as if to exclude less water from the crevices and interiors of proteins, than the MS model. Such behavior was anticipated, given the sensitivity of the dielectric function to local details of protein structure, and the tendency to ascribe to void like regions inaccessible to discrete water, dielectric values higher that found in the molecular interior. This behavior

of macromolecular solvation was hoped for in the continuous model because of the prior observation that the discrete MS boundary leads to a model of protein residues that is unrealistically difficult to desolvate. A high dielectric constant for the protein in the MS model reduces the desolvation penalty. This is one factor that accounts for the widespread adoption of a dielectric constant of 4 in PB approaches to calculate pKa values and binding energies. In contrast, experimental measurements on a wide range of organic liquids reveal a fundamental dielectric of around 2. A key feature of the continuous model is that for proteins, the interior of atoms are assigned values of the fundamental dielectric, whereas the overall solvation behavior is broadly comparable to the discrete model using a protein dielectric constant of 4. This similarity in models was observed for calculations of desolvation energies, pKa shifts, and binding energies. Despite the simplicity of the treatment of pKa shifts and binding energies, both of these protein solvation models produced predictions in accord with the experiment. However, the continuous model provides a simple and unified description of the dielectric of the atomic interior for both small and macromolecular systems. This consistent description is especially important in PB approaches to the binding energy problem. In the MS model different dielectric values best characterize the atomic interiors of small and macromolecular systems. This necessitates *ad hoc* assumptions about the best description of small molecule dielectric values, and solvation behavior in aqueous and protein binding pocket environments. The continuous model does not suffer such drawbacks.

The algorithmic advantages of the continuous model have been clearly demonstrated in this work. The underlying representation of atom-centered Gaussians ensures that the generation of accurate dielectric maps is computationally efficient. This eliminates a potential bottleneck in solving the PBe. Orientational and grid scale errors are smaller using the smooth dielectric function. This has been quantified in detail for small molecule solvation energies, and illustrated graphically in the case of protein–protein binding energies (see Figs. 12 and 13). Such improved precision is essential for calculating protein–ligand binding energies. A more detailed analysis of errors in the binding energy problem will subsequently appear.

A key motivation in introducing an analytical, smooth dielectric function, is the simplification in obtaining solvent forces in the context of the PBe. Specifically, electrostatic forces that arise from the presence of a dielectric transition region are trivial to obtain (unlike their MS counterparts). In addition, because the smooth function directly ties atomic movements to changes in the dielectric, discontinuities that arise in the MS model from vanishing cavities are eliminated. This is also true of the IVC approach of Friesner et al.[9] These authors use a discontinuous dielectric to obtain solvation energies and forces, but with a sophisticated finite element technique using an adaptive nonregular grid. The latter is a device for reducing errors associated with the discrete dielectric boundary. However, a thorough comparison with our own work is not possible because of the lack of error analysis given in their article. The continuous function introduced in our work has led to precise computation of solvent forces, for small molecules. The method scales well for larger systems, as demonstrated by the application to the optimization of proteins. Given our method's speed and facile derivative, it is interesting to compare it to the fast empirical Generalized Born (GB) method. GB achieves accuracy relative to high-resolution PBe of about 10%. Although we have not demonstrated such, it is likely that there will be little performance penalty in using ZAP at a grid scale that gives comparable precision. In addition, although GB allows fast calculation of forces, it does not scale well to large systems, unlike ZAP. On the other hand, second derivatives are hard for our method, but easy for GB. Finally, GB has more recently been applied to the protein–ligand binding problem,[67] whereas PBe has been regarded as too slow and inaccurate, neither of which is now true. Also, GB includes assumptions as to the desolvation of concave protein pockets, which are manifestly incorrect. Essentially, field lines are assumed rectilinear from any embedded charges, which any study with a visualization program such as GRASP[68] will indicate is wrong. There has been little study to date as to the consequence of such assumptions, from which our approach remains free.

In conclusion, we have incorporated a smooth dielectric function into PB technology, and demonstrated that such a method retains the predictive ability of established approaches. The approach offers a consistent description of both small and macromolecular systems, and considerable algorithmic advances in accuracy, performance and the ability to obtain forces.

Appendix A: Mathematical Background

This Appendix is intended to present equations in a consistent system of SI units,[69] and introduce a

consistent notation referred to extensively throughout our work.

We begin by assuming the existence of a continuous dielectric that is spatially inhomogeneous, and that surrounds a time-independent charge density $\rho(\mathbf{r})$, where the vector $\mathbf{r}$ with components r_α, $(\alpha = x, y, z)$ denotes the position inside the system. The electric displacement vector $D_\alpha(\mathbf{r})$ is determined from Maxwell's first equation

$$\nabla_\alpha D_\alpha = \rho(\mathbf{r}) \tag{27}$$

In this Appendix we adopt the Einstein summation convention that repeated Greek indices are summed over. The electric displacement is related to the applied electric field $E_\alpha(\mathbf{r})$ using the permittivity tensor

$$D_\alpha(\mathbf{r}) = \epsilon_{\alpha\beta}(\mathbf{r})E_\beta \tag{28}$$

In the present work we assume that the permittivity is isotropic, i.e.,

$$\epsilon_{\alpha\beta}(\mathbf{r}) = \delta_{\alpha\beta}\epsilon(\mathbf{r}) \tag{29}$$

Using the scalar potential

$$E_\alpha(\mathbf{r}) = -\nabla_\alpha\phi(\mathbf{r}) \tag{30}$$

and substituting into eq. (28) we obtain

$$\nabla_\alpha\{\epsilon(\mathbf{r})\nabla_\alpha\phi(\mathbf{r})\} = -\rho(\mathbf{r}) \tag{31}$$

The charge density, $\rho(\mathbf{r})$, can be divided into two parts: (i) a contribution (ρ_{mol}) from partially charged atoms or groups of atoms within molecules; and (ii) a contribution (ρ_{ion}) from "mobile" ions distributed in the electrolyte solvent.

The difference between (i) and (ii) is that charges contributing to (i) are to be treated explicitly, whilst charges in (ii) are treated as part of the statistical model contributing to the continuum background. Hence, we write

$$\rho(\mathbf{r}) = \rho_{mol}(\mathbf{r}) + \rho_{ion}(\mathbf{r}) \tag{32}$$

The ion distribution is treated using the Debye–Hückel model, in which each ion is surrounded by a screening atmosphere of counterions. Assuming for simplicity an electrolyte of ions with charges z_+e and z_-e ($z_+ = -z_-$) then

$$\rho_{ion}(\mathbf{r}) = e\{z_+n_+(\mathbf{r}) + z_-n_-(\mathbf{r})\} \tag{33}$$

The quantities $n(\mathbf{r})$ are cation/anion number densities. According to the Debye–Hückel model the tendency for any particular ion to attract counterions is governed by purely coulombic interactions, balanced by thermal disruption, and assumes that the local ion number densities are given by a Boltzmann distribution thus:

$$n_\pm(\mathbf{r}) = \lambda(\mathbf{r})n_\pm^0 \exp\left\{\frac{-z_\pm e\phi(\mathbf{r})}{kT}\right\} \tag{34}$$

where $z_\pm e\phi(\mathbf{r})$ is the energy of an ion in the total potential $\phi(\mathbf{r})$ of the system, $n_\pm^0$ is the bulk value of the ion number density, more conveniently expressed in terms of molality, thus:

$$n_\pm^0 = m_\pm N_A\rho_0 \tag{35}$$

where $m_\pm$ is the ion molality, N_A is Avogadro's constant, and ρ_0 is the solvent density. The distribution function (34) contains a masking function $\lambda(\mathbf{r})$ usually given by a simple unit step function, which models the Stern layer. The Stern layer is a region around the solute from which ions are excluded ($n_\pm = 0$) and accounts in an approximate way for the finite size of solvated ions. In the present work, the unit-step function will be replaced by an analytic function to describe the Stern layer, the details of which are given in eq. (7) of the Methods section. The electrical neutrality condition ($z_+n_+^0 + z_-n_-^0 = 0$) can be used to obtain

$$\rho_{ion}(\mathbf{r}) = \lambda(\mathbf{r})n_+^0 e\left\{z_+\exp\left(\frac{-z_+e\phi}{kT}\right) + z_-\exp\left(\frac{-z_-e\phi}{kT}\right)\right\} \tag{36}$$

which for counterions of equal and opposite charges leads to

$$\rho_{ion}(\mathbf{r}) = -2\lambda(\mathbf{r})z_+n_+^{(0)}e\sin h\left(\frac{z_+e\phi}{kT}\right) \tag{37}$$

which can be substituted into (31) and (32) to give the nonlinear PBe

$$\nabla_\alpha\{\epsilon(\mathbf{r})\nabla_\alpha\phi(\mathbf{r})\} + \lambda(\mathbf{r})\kappa^2\sin h\left(\frac{z_+e\phi}{kT}\right) = -\rho_{mol}(\mathbf{r}) \tag{38}$$

where the constant κ is

$$\kappa = [2ez_+m_+N_A\rho_0]^{1/2} \tag{39}$$

Expansion of (37) in powers of $z_\pm\phi/kT$ gives the linearized PBe

$$\nabla_\alpha\{\epsilon(\mathbf{r})\nabla_\alpha\phi(\mathbf{r})\} + \lambda(\mathbf{r})\kappa_0^2\phi(\mathbf{r}) = -\rho_{mol} \tag{40}$$

where the constant

$$\kappa_0 = \left\{\frac{2e^2N_A\rho_0I}{kT}\right\} \tag{41}$$

and the ionic strength

$$I = \tfrac{1}{2}(m_+z_+^2 + m_-z_-^2) \tag{42}$$

DISCRETIZATION OF THE POISSON–BOLTZMANN EQUATION

The finite difference methodology for obtaining numerical solutions to the PBe, relies upon a mapping of the physical quantities described in Appendix B, onto a grid. Differences in these mapped grid values replace differential operators appearing in equations such as (38) and (40). This standard numerical treatment is well known, and the purpose of the following section is merely to introduce notation and equations relevant to our goal of introducing a more convenient set of analytic mapping functions for the dielectric tensor, charge density, and ionic boundary (Stern Layer), and describing the computation of solvent forces.

We begin by introducing a rectangular grid indexed by integers i, j, k, with grid points at

$$\mathbf{R}_{ijk} = \mathbf{R}_0 + i\mathbf{e}_1 + j\mathbf{e}_2 + k\mathbf{e}_3 \tag{43}$$

where $\mathbf{e}_1$, $\mathbf{e}_2$, and $\mathbf{e}_3$ are mutually orthogonal vectors of length h_1, h_2, and h_3, respectively. The vector $\mathbf{R}_0 = (X_0, Y_0, Z_0)$ can be considered as a grid origin vector. An important consideration of numerical solutions to the PBe is the stability of the solution with respect to

- size of h_1, h_2, h_3 (grid scale dependence)
- variation of the directions of the axes $\mathbf{e}_1$, $\mathbf{e}_2$, $\mathbf{e}_3$ (rotational variance)
- variation of the grid origin, $\mathbf{R}_0$ (translational variance)

In what follows, a general scalar field $f(x, y, z)$ at a grid point is denoted by

$$f_{ijk} = f(\mathbf{R}_{ijk}) \tag{44}$$

Surrounding each grid point (i, j, k) we inscribe a parallelepiped "unit cell" of volume $h_1h_2h_3$ defined by:

$$\begin{aligned} V_{ijk}: \quad & \left(i - \tfrac{1}{2}\right)h_1 \le x - X_0 \le \left(i + \tfrac{1}{2}\right)h_1 \\ & \left(j - \tfrac{1}{2}\right)h_2 \le y - Y_0 \le \left(j + \tfrac{1}{2}\right)h_2 \\ & \left(k - \tfrac{1}{2}\right)h_3 \le z - Z_0 \le \left(k + \tfrac{1}{2}\right)h_3 \end{aligned}$$

The unit cell is bounded by six faces $S_{i\pm1/2}$, $S_{j\pm1/2}$, and $S_{k\pm1/2}$, which are perpendicular to the $\mathbf{e}_1$, $\mathbf{e}_2$, and $\mathbf{e}_3$ directions at the respective $\frac{1}{2}$ grid spacings. From the definition of the electric displacement vector

$$\mathbf{D}(\mathbf{r}) = \epsilon(\mathbf{r})\nabla\phi(\mathbf{r}) \tag{45}$$

the linearized PB eq. (40) becomes

$$\nabla \cdot \mathbf{D} + \kappa_0^2\phi = -\rho_{mol} \tag{46}$$

Integrating both sides of eq. (46) inside the unit cell V_{ijk} gives

$$\int_{V_{ijk}} d\mathbf{r}\, \nabla \cdot \mathbf{D} + \kappa_0^2 \int_{V_{ijk}} d\mathbf{r}\, \phi(\mathbf{r}) = -\int_{V_{ijk}} d\mathbf{r}\, \rho_{mol}(\mathbf{r}) \tag{47}$$

The solute charge inside the unit cell is defined as

$$q_{ijk} = \int_{V_{ijk}} d\mathbf{r}\, \rho_{mol}(\mathbf{r}) \tag{48}$$

The details of mapping discrete charge distributions onto the grid are discussed in the Methods section. The first term of eq. (47) can be simplified using Gauss' theorem to obtain a set of integrals over the face of the "unit cell," thus:

$$\int_{V_{ijk}} d\mathbf{r}\, \nabla \cdot \mathbf{D} = \sum_{faces,n} \int d\mathbf{S}_n \cdot \mathbf{D}(\mathbf{r}) \tag{49}$$

Considering a single face $S_{i+1/2}$ as an example

$$\int d\mathbf{S}_{i+1/2} \cdot \mathbf{D}(\mathbf{r}) = \int_{(Y_0+j-1/2)h_2}^{(Y_0+j+1/2)h_2} dy \int_{(Z_0+k-1/2)h_3}^{(Z_0+k+1/2)h_3} dz\, \mathbf{n} \cdot \mathbf{D}\left(\left(X_0 + i + \tfrac{1}{2}\right)h_1, y, z\right) \tag{50}$$

The electric displacement vector field at face $S_{i+1/2}$:

$$\mathbf{D}_x\left(\left(X_0 + i + \tfrac{1}{2}\right)h_1, y, z\right)\Big|_{S_{i+1/2}} = \epsilon\left(\left(X_0 + i + \tfrac{1}{2}\right)h_1, y, z\right) \times \nabla_x\phi\left(\left(X_0 + i + \tfrac{1}{2}\right)h_1, y, z\right) \tag{51}$$

must now be expressed in terms of appropriate grid quantities. This is achieved by assuming

$$\epsilon\left(\left(X_0 + i + \tfrac{1}{2}\right)h_1, y, z\right)\Big|_{S_{i+1/2}} \simeq \epsilon_{i+1/2jk} \tag{52}$$

that is, ϵ is evaluated at the center of the face, and assumed to be constant over the whole face. Similarly

$$\nabla_x\phi\left(\left(X_0 + i + \tfrac{1}{2}\right)h_1, y, z\right)\Big|_{S_{i+1/2}} \simeq (\phi_{i+1jk} - \phi_{ijk})\frac{1}{h_1} \tag{53}$$

where the gradient in the outward face direction is taken as the point of numerical differentiation, and assumed to be constant over the face $S_{i+1/2}$. The integral (50) is given by:

$$\int d\mathbf{S}_{i+1/2} \cdot \mathbf{D}(\mathbf{r}) \simeq \left(\frac{h_2h_3}{h_1}\right)\epsilon_{i+(1/2)jk}(\phi_{i+1jk} - \phi_{ijk}) \tag{54}$$

The remaining face integrals can be simplified in the same way. The ionic strength term is written as the cell volume integral

$$\kappa_0^2 \int_{V_{ijk}} d\mathbf{r}\, \lambda(\mathbf{r})\phi(\mathbf{r}) \tag{55}$$

which has to be approximated by assuming that $\lambda(\mathbf{r})$ and $\phi(\mathbf{r})$ are constant and at their central grid values over the whole cell. Hence, (55) becomes

$$\kappa_0^2 \lambda_{ijk} \phi_{ijk} h_1 h_2 h_3 \tag{56}$$

In this way the linearized PBe can be written as a set of linear matrix equations

$$\sum_{i'j'k'} A_{i'j'k'} \Phi_{i'j'k'} = q_{ijk} \qquad \forall_{ijk} \tag{57}$$

where the nonzero elements of the **A** matrix are defined according to:

$$\begin{aligned}
A_{ijk,ijk} &= \left(\frac{h_2 h_3}{h_1}\right)\{\epsilon_{i-(1/2)jk} + \epsilon_{i+(1/2)jk}\} \\
&\quad + \left(\frac{h_3 h_1}{h_2}\right)\{\epsilon_{ij-(1/2)k} + \epsilon_{ij+(1/2)k}\} \\
&\quad + \left(\frac{h_1 h_2}{h_3}\right)\{\epsilon_{ijk-1/2} + \epsilon_{ijk+1/2}\} \\
&\quad + (h_1 h_2 h_3)\kappa_0^2 \lambda_{ijk} \\
A_{ijk,i-1jk} &= -\left(\frac{h_2 h_3}{h_1}\right)\epsilon_{i-(1/2)jk} \\
A_{ijk,i+1jk} &= -\left(\frac{h_2 h_3}{h_1}\right)\epsilon_{i+(1/2)jk} \\
A_{ijk,ij-1k} &= -\left(\frac{h_3 h_1}{h_2}\right)\epsilon_{ij-(1/2)k} \\
A_{ijk,ij+1k} &= -\left(\frac{h_3 h_1}{h_2}\right)\epsilon_{ij+(1/2)k} \\
A_{ijk,ijk-1} &= -\left(\frac{h_1 h_2}{h_3}\right)\epsilon_{ijk-1/2} \\
A_{ijk,ijk+1} &= -\left(\frac{h_1 h_2}{h_3}\right)\epsilon_{ijk+1/2}
\end{aligned} \tag{58}$$

It is obvious that the **A** matrix is hermitian since

$$\begin{aligned}
A_{i-1jk,ijk} &= -\left(\frac{h_2 h_3}{h_1}\right)\epsilon_{i-(1/2)jk} \\
&= A_{ijk,i-1jk}
\end{aligned} \tag{59}$$

The matrix equations in (57) can be solved by applying approximated boundary conditions and using standard iterative techniques. The computation of solvent forces using eq. (22) requires the calculation of the derivatives of the **A** matrix in (58) and (59). This can be carried out explicitly at each grid point (ijk) because ϵ and λ have simple analytic forms.

Appendix B: Quadratic Inverse-Interpolation

We introduce the relevant notation and mathematics by considering the simple inverse-linear interpolation in one dimension.

For a charge Q at $\mathbf{R} = (X, Y, Z)$ we define a dimensionless x coordinate relative to the grid origin at X_0, and the grid spacing h_1 as $x = (X - X_0)/h_1$. For $i \le x \le i+1$ the charge is apportioned to nodes i and $(i+1)$ in the ratio $(x-1)/(i+1-x)$ while conserving the total charge. Hence,

$$\left.\begin{aligned} q_i &= Q(i+1-x) \\ q_{i+1} &= Q(x-i) \end{aligned}\right\} \; i \le x \le i+1 \tag{60}$$

This linear scheme leads to a saw tooth (with discontinuous first derivatives) variation in charge at node i, as x varies across the whole grid. The variation in charge at each node can be expressed in terms of a second order basis spline[70] thus:

$$q_i(x) = Q N_{i-1}^{(2)}(x) \tag{61}$$

where we introduce the following notation to describe the basis spline:

$$N_{i-1}^{(2)} = \begin{cases} (i+1-x) & i \le x \le (i+1) \\ x-(i-1) & (i-1) \le x \le i \\ 0 & \forall \text{ other } x \end{cases} \tag{62}$$

In particular, eq. (62) satisfies two important conditions, namely

$$q_i + q_{i+1} = Q \tag{63}$$

which is charge conservation, and

$$i q_i + (i+1) q_{i+1} = Q x \tag{64}$$

which is conservation of dipole moment. In addition, (62) is differentiable with respect to the parameter X. In three dimensions we simply obtain:

$$q_{ijk}(\mathbf{R}) = Q N_{i-1}^{(2)}(x) N_{j-1}^{(2)}(y) N_{k-1}^{(2)}(z) \tag{65}$$

In terms of smoothness, q_{ijk} is continuous, and has well defined, but discontinuous first derivatives. A smoother inverse interpolation of charges onto grid points is now described, which involves a quadratic sharing of charge between three nearest grid points. Using the notation described for the linear case we find:

$$\begin{aligned}
q_i(x) &= Q\left\{\tfrac{3}{4} - (x-i)^2\right\} \\
q_{i+1}(x) &= Q\left\{\tfrac{1}{8} + \tfrac{1}{2}(x-i) + \tfrac{1}{2}(x-i)^2\right\} \\
q_{i-1}(x) &= Q\left\{\tfrac{1}{8} - \tfrac{1}{2}(x-i) + \tfrac{1}{2}(x-i)^2\right\}
\end{aligned} \tag{66}$$

for $\frac{1}{2} \le x \le i + \frac{1}{2}$ (i.e., for cell i). These formulae also satisfy charge and dipole moment conservation. The

charge on a single node at all x is given by:

$$q_i = Q \times \begin{cases} \frac{1}{8} + \frac{1}{2}(x - i + 1) + \frac{1}{2}(x - i + 1)^2 \\ \qquad i - \frac{3}{2} \le x \le i - \frac{1}{2} \\ \frac{3}{4} - (x - i)^2 \\ \qquad i - \frac{1}{2} \le x \le i + \frac{1}{2} \\ \frac{1}{8} - \frac{1}{2}(x - i - 1) + \frac{1}{2}(x - i - 1)^2 \\ \qquad i + \frac{1}{2} \le x \le i + \frac{3}{2} \end{cases} \tag{67}$$

or in spline notation:

$$q_i = QN^{(3)}_{i-1/2}(x) \tag{68}$$

where $N^{(3)}_{i-1/2}(x)$ is the third order (quadratic) basis spline. The full interpolation formula in three dimensions is simply:

$$q_{ijk}(\mathbf{R}) = QN^{(3)}_{i-1/2}(x)N^{(3)}_{j-1/2}(y)N^{(3)}_{k-1/2}(z) \tag{69}$$

which also satisfies the charge and dipole conservation condition as before. This quadratic interpolation is continuous, and has continuous first derivatives, but discontinuous second derivatives. It is possible to extend the hierarchy by considering higher order basis spline functions, but that is not considered further in this work. It is easy to recognize that quantities computed on a grid by solution of the PBe can be calculated at fixed points such as atom centers by the application of standard direct spline interpolation.

Acknowledgments

We acknowledge the expert assistance of Christine Kitchen, in the graphing and analysis of the data, and would like to thank Brooke Magnanti for linguistic advice. We are grateful to Sandra McLaughlin for her expertise in writing a number of Perl scripts, used in many of the calculations in this article, and to Sue Margetson for help in preparation of the diagrams. We also thank Dave Timms for many helpful discussions and making available results on the binding energy problem.

References

1. Nicholls, A. www.eyesopen.com.
2. Gilson, M.; Sharp, K. A.; Honig, B. J Comput Chem 1987, 9, 327.
3. Sharp, K.; Honig, B. Annu Rev Biophys Chem 1990, 19, 301.
4. Bell, R. P. Trans Faraday Soc 1931, 27, 797.
5. Born, M. Zeit Physik 1920, 1, 79.
6. Onsager, L. J Am Chem Soc 1936, 58, 1486.
7. Richards, F. M. Annu Rev Biophys Bioeng 1977, 6, 151.
8. Lee, B.; Richards, F. M. J Mol Biol 1971, 55, 151.
9. Friedrichs, M.; Zhou, R.; Edinger, S. R.; Friesner, R. A. J Phys Chem B 1999, 103, 3057.
10. Cortois, C. M.; Friesner, R. A. J Comput Chem 1997, 18, 1570.
11. Cortois, C. M.; Friesner, R. A. J Comput Chem 1997, 18, 1591.
12. Zauhar, R.; Morgan, R. J. J Mol Biol 1985, 186, 815.
13. Vorobjev, Y. N.; Grant, J. A.; Scheraga, H. A. J Am Chem Soc 1992, 114, 898.
14. Bharadwaj, R.; Windemuth, A.; Nicholls, A.; Sridharan, S.; Honig, B. J Comput Chem 1995, 16, 898.
15. Nicholls, A. J Comput Chem 1991, 12, 435.
16. Holst, M.; Saied, F. J Comput Chem 1993, 14, 105.
17. Holst, M.; Kozack, R. E.; Saied, F.; Subramaniam, S. Protein Struct Func Genet 1994, 18, 231.
18. Davis, M. E.; McCammon, J. A. J Comput Chem 1991, 12, 909.
19. Bruccoleri, R. E.; Novotony, J.; Davis, M. E.; Sharp, K. J Comput Chem 1997, 18, 268.
20. Grant, J. A.; Pickup, B. T. J Phys Chem 1995, 99, 3503.
21. Grant, J. A.; Pickup, B. T. Computer Simulation of Biomolecular Systems; Kluwer/ESCOM: New York, 1998; pp. 150–176, vol. 3.
22. Gibson, K. D.; Scheraga, H. A. Mol Phys 1987, 62, 1247.
23. Kitts, P. PhD thesis, University of Sheffield, 1998.
24. Schaefer, M.; Karplus, M. J Phys Chem 1996, 100, 1578.
25. Still, W. C.; Tempczyk, A.; Hawley, R. C.; Hendrickson, T. J Am Chem Soc 1990, 112, 6127.
26. Im, W.; Beglov, D.; Roux, B. Comput Phys Commun 1998, 11, 59.
27. Gilson, M. K.; Davis, M. E.; Luty, B. A.; McCammon, J. A. J Phys Chem 1993, 97, 3591.
28. Klapper, I.; Hagstrom, R.; Fine, R.; Sharp, K.; Honig, B. Protein Struct Funct Genet 1986, 1, 47.
29. Bruccoleri, R. E. J Comput Chem 1993, 14, 1417.
30. McWeeny, R. Methods of Molecular Quantum Mechanics; Academic Press Inc.: San Diego, CA, 1992.
31. Luty, B. A.; Davis, M. E.; McCammon, J. A. J Comput Chem 1992, 13, 768.
32. Allen, F. H.; Davies, J. E.; Galloy, J. J.; Johnson, O.; Kennard, O.; Macrae, C. F.; Mitchell, E. M.; Mitchell, G. F.; Smith, J. M.; Watson, D. G. J Chem Inf Comp Sci 1991, 31, 187.
33. Allen, F. H.; Kennard, O. Chem Design Automat News 1993, 8, 31.
34. InsightII User Guide; Biosym/MSI: San Diego, 1995.
35. Vesely, F. J. J Comput Phys 1982, 47, 291.
36. Marsaglia, A. Annu Math Stat 1972, 43, 645.
37. Kitchen, C.; Pickup, B. T.; Grant, J. A.; Nicholls, A. in preparation.
38. Rashin, A. A.; Honig, B. J Phys Chem 1985, 89, 5588.
39. Hahn, M. J Med Chem 1995, 38, 2080.
40. Dudek, M. J.; Ramnarayan, K.; Ponder, J. W. J Comput Chem 1998, 19, 548.
41. Roterman, I. K.; Gibson, K. D.; Scheraga, H. A. J Biomol Struct Dynam 1989, 7, 391.
42. Madison, V.; Kopple, D. J Am Chem Soc 1980, 102, 4855.
43. Bernstein, F. C.; Koetzle, T. F.; Williams, G. J. B.; Meyer, E. F., Jr.; Brice, M. D.; Rodgers, J. R.; Kennard, O.; Shimanouchi, T.; Tasumi, M. J Mol Biol 1977, 112, 535.

44. MacKerell, A. D.; Bashford, D.; Bellott, M.; Dunbrack, R. L.; Evanseck, J. D.; Field, M. J.; Fischer, S.; Gao, J.; Guo, H.; Ha, S.; Joseph-McCarthy, D.; Kuchnir, L.; Kuczera, K.; Lau, F. T. K.; Mattos, C.; Michnick, S.; Ngo, T.; Nguyen, D. T.; Prodhom, B. W. E.; Reiher, I.; Roux, B.; Schlenkrich, M.; Smith, J. C.; Stote, R.; Straub, J.; Watanabe, M.; Wiorkiewicz-Kuczera, J.; Yin, D.; Karplus, M. J Phys Chem B 1998, 102, 3586.
45. Gilson, M.; Honig, B. Biopolymers 1986, 25, 2097.
46. Gilson, M. Computer Simulation of Biomolecular Systems; Kluwer/ESCOM: New York, 1998; vol. 3, pp. 199–220.
47. Russell, S. T.; Warshel, A. J Mol Biol 1985, 185, 389.
48. Warshel, A.; Sussman, F.; King, G. Biochemistry 1986, 25, 8368.
49. Bashford, D.; Karplus, M. Biochemistry 1990, 29, 10219.
50. Bashford, D.; Karplus, M. J Phys Chem 1991, 95, 9556.
51. Yang, A. S.; Gunner, M. R.; Sampogna, R.; Sharp, K.; Honig, B. Proteins Struct Funct Genet 1993, 15, 252.
52. Antosiewicz, J.; McCammon, J. A.; Gilson, M. K. J Mol Biol 1994, 238, 415.
53. Alexov, E. G.; Gunner, M. R. Biophys J 1997, 74, 2075.
54. Beroza, P.; Fredkin, D. R.; Okamura, M. Y.; Feher, G. Proc Natl Acad Sci USA 1991, 88, 5804.
55. Shen, J.; Quiocho, F. A. J Comput Chem 1995, 16, 445.
56. Mistra, V. K.; Honig, B. Proc Natl Acad Sci USA 1995, 92, 4691.
57. Froloff, N.; Windemuth, A.; Honig, B. Protein Sci 1997, 6, 1293.
58. Gilson, M. K.; Honig, B. Protein Struct Funct Genet 1988, 4, 7.
59. Hedstrom, L.; Lin, T. Y.; Fast, W. Biochemistry 1996, 35, 4515.
60. Hermann, R. B. J Phys Chem 1971, 76, 2754.
61. Chothia, C. J Mol Biol 1976, 105, 1.
62. Timms, D.; Birch, L. in preparation.
63. Shuker, S. B.; Hajduk, P. J.; Meadoes, R. P.; Fesik, S. W. Science 1996, 274, 1531.
64. Tsai, F.; Singh, P. O. M.; Skarzynski, T.; Wonacott, A. J.; Weston, S.; Tucker, A.; Pauptit, R. A.; Breeze, A. L.; Poyser, J. P.; O'Brien, R.; Ladbury, J. E.; Wigley, D. B. Protein Struct Funct Genet 1997, 28, 41.
65. Ponder, J. Software Tools for Molecular Design, Version 3.7; Washington University School of Medicine: St. Louis, 1999.
66. Braun, W. Computer Simulation of Biomolecular Systems; Kluwer/ESCOM: New York, 1998; vol. 3, pp. 270–283.
67. Zou, X.; Sun, Y.; Kuntz, I. D. J Am Chem Soc 1999, 121, 8033.
68. Nicholls, A.; Sharp, K. A.; Honig, B. Protein Struct Funct Genet 1991, 11, 281.
69. Mills, I.; Cvitas, T.; Homann, K.; Kallay, N.; Kuchitsu, K. Quantities, Units and Symbols in Physical Chemistry; Blackwell Scientific Publications: Oxford, 1993.
70. Schumaker, L. L. Spline Functions: Basic Theory; Wiley: New York, 1981.
71. Antosiewicz, J.; McCammon, J. A.; Gilson, M. K. Biochemistry 1996, 35, 7819.